Science Advances
AAAS

Supplementary Materials for

Adolescence is a sensitive period for prefrontal microglia to act on cognitive development

Sina M. Schalbetter, Anina S. von Arx, Natalia Cruz-Ochoa, Kara Dawson, Andranik Ivanov, Flavia S. Mueller, Han-Yu Lin, René Amport, Wiebke Mildenberger, Daniele Mattei, Dieter Beule, Csaba Földy, Melanie Greter, Tina Notter, Urs Meyer*

*Corresponding author. Email: urs.meyer@vetpharm.uzh.ch

Published 2 March 2022, *Sci. Adv.* **8**, eabi6672 (2022)
DOI: 10.1126/sciadv.abi6672

This PDF file includes:

Supplementary Figures and Tables

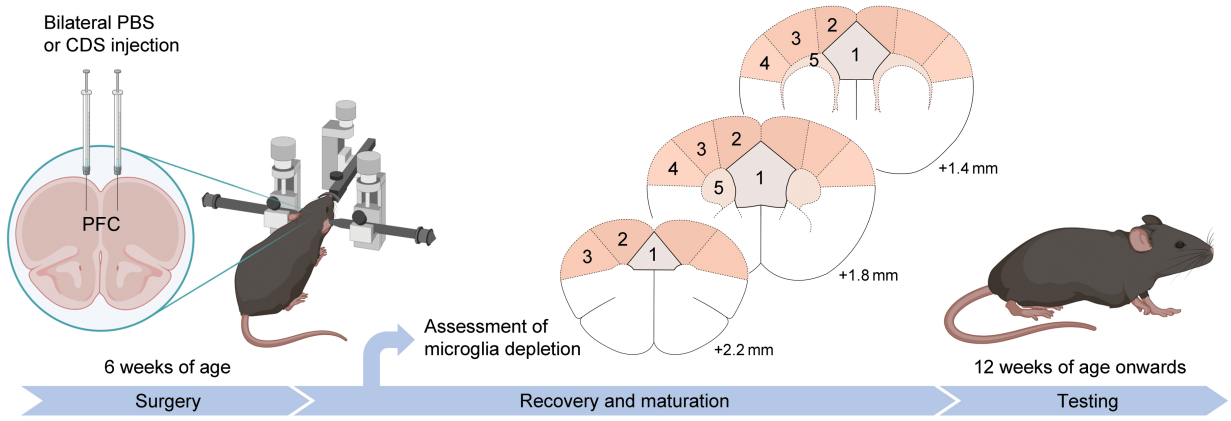

Fig. S1. Main experimental design of the study. To deplete microglia selectively and transiently from the prefrontal cortex during a defined window of adolescence, 6-week-old C57BL6/N male mice received a single, bilateral stereotaxic injection of clodronate disodium salt (CDS) into the prefrontal cortex (PFC). Control mice received a bilateral stereotaxic injection of phosphate-buffered saline (PBS). An additional group of mice receiving sham surgery, which involved the same surgical procedures but no stereotaxic injections, was included as a negative control group as well (not depicted in the figure). The magnitude and specificity of microglia depletion was ascertained by post-mortem immunohistochemistry in the PFC (1), secondary motor cortex (2), primary motor cortex (3), primary somatosensory cortex (4), and forceps minor of the corpus callosum (5) along the anterior (bregma +2.2. mm) to posterior (bregma +1.4 mm) axis, which was conducted at successive time points (1, 5, 10, and 20 days post-injection [dpi]) after CDS or PBS injection or sham surgery. To test the effects of adolescent PFC microglia depletion on adult behavioral and synaptic functions, 6-week-old C57BL6/N male mice received a single, bilateral stereotaxic injection of CDS or PBS into PFC and were then allowed to recover and mature into adulthood. Adult testing commenced at 12 weeks of age.

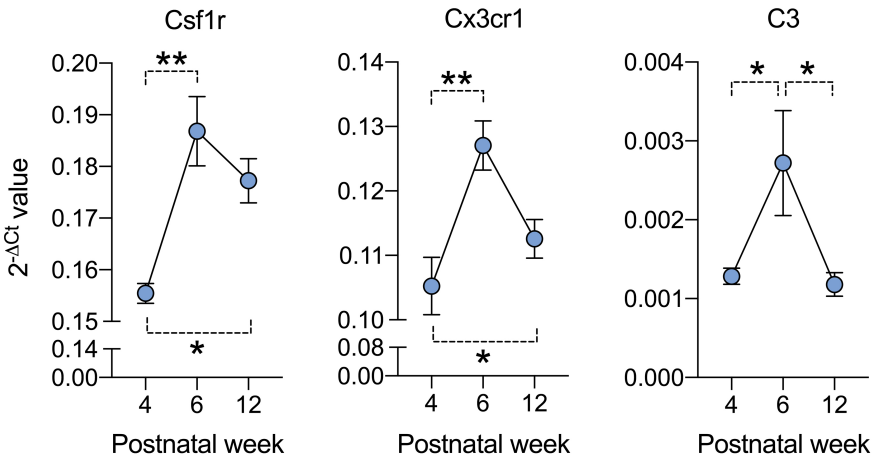

Fig. S2. Basal Expression of microglia-defining and complement component genes in the PFC of mice across preadolescence to adulthood. Basal expression of microglia-defining genes (Csf1r and Cx3cr1) and complement component 3 (C3) was assessed in PFC samples obtained from preadolescent (4-week-old), adolescent (6-week-old) and adult (12-week-old) male C57BL6/N mice using quantitative real-time polymerase chain reaction (qRT-PCR). *$p < 0.05$ and **$p < 0.01$, based on Tukey's multiple comparison post-hoc test following ANOVA (Csf1r: $F_{(2,12)} = 11.6$, $p < 0.01$; Cx3cr1: $F_{(2,12)} = 8.3$, $p < 0.01$; C3: $F_{(2,12)} = 4.7$, $p < 0.05$); $N = 5$ mice per postnatal week.

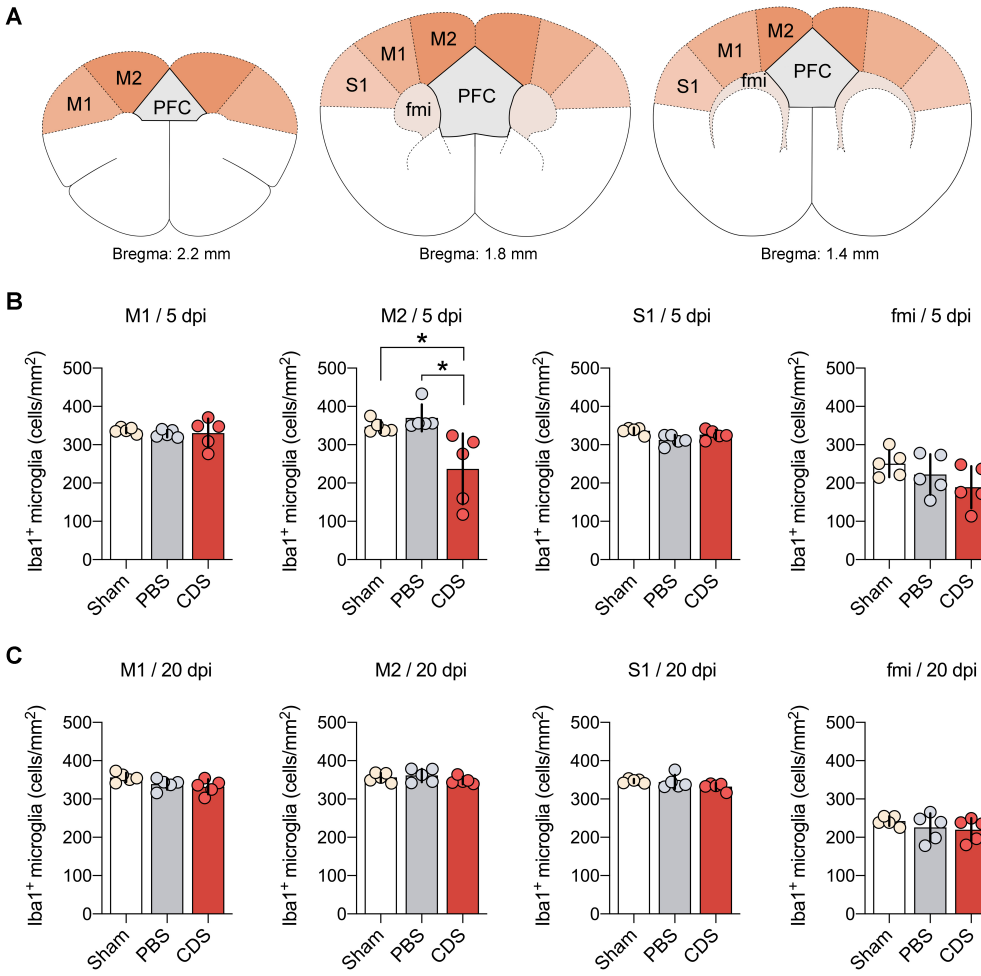

Fig. S3. CDS-induced microglia depletion in brain areas bordering the PFC of adolescent mice. **(A)** Post-mortem immunohistochemistry was used to assess CDS-induced microglia depletion in the brain areas bordering the PFC of adolescent mice. As illustrated in the schematic coronal sections, the bordering areas included primary motor cortex (M1), secondary motor cortex (M2), primary somatosensory cortex (S1), and forceps minor of the corpus callosum (fmi) along the anterior (bregma +2.2. mm) to posterior (bregma +1.4 mm) axis. **(B)** The bar plots show the number of Iba1$^+$ microglia in M1, M2, S1 and fmi regions of sham control mice, PBS control mice and CDS mice at 5 dpi, which corresponds to the peak of microglia depletion in the PFC of adolescent males injected with CDS (see *Figure 1* in main text). *$p <$ 0.05, based on post-hoc test following ANOVA ($F_{(2,12)} = 7.6$, $p < 0.01$). **(C)** The bar plots depict the number of Iba1$^+$ microglia in M1, M2, S1 and fmi regions of sham control mice, PBS control mice and CDS mice at 20 dpi, which corresponds to a post-injection interval when microglia density is fully restored in the PFC of adolescent males injected with CDS (see *Figure 1* in main text). All data are means ± SEM with individual values overlaid; $N = 5$ mice per group and dpi.

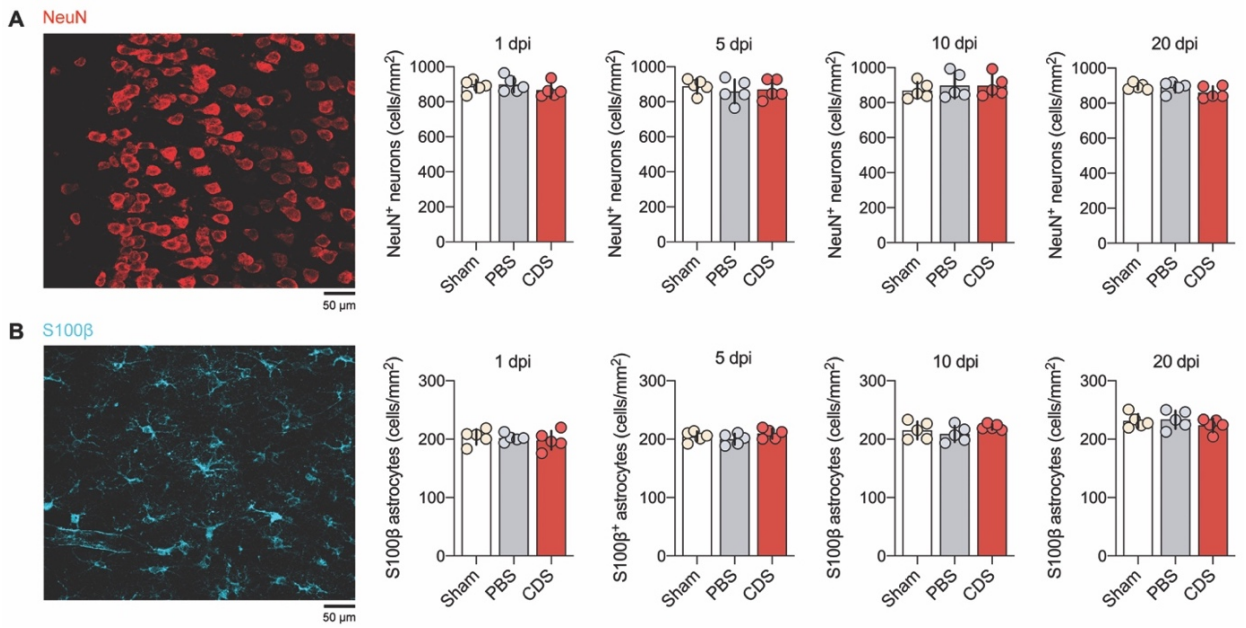

Fig. S4. Density of neurons and astrocytes in the PFC after sham, PBS or CDS treatment in adolescent mice. Post-mortem immunohistochemistry was used to assess whether bilateral stereotaxic injection of CDS into the PFC of adolescent mice alters the density of neurons and astrocytes, which were stained using anti-NeuN and anti-S100β antibody, respectively. **(A)** The photomicrograph shows a representative NeuN immunofluorescent stain in the PFC region. The bar plots depict the number of $NeuN^+$ neurons in the PFC of sham control mice, PBS control mice and CDS mice at different days post-injection (dpi). There were no group differences with regards to the density of $NeuN^+$ neurons at any dpi. **(B)** The photomicrograph shows a representative S100β immunofluorescent stain in the PFC region. The bar plots depict the number of $S100\beta^+$ astrocytes in the PFC of sham control mice, PBS control mice and CDS mice at different dpi intervals. There were no group differences with regards to the density of $S100\beta^+$ astrocytes at any dpi. All data are means ± SEM with individual values overlaid; $N = 5$ mice per group and dpi.

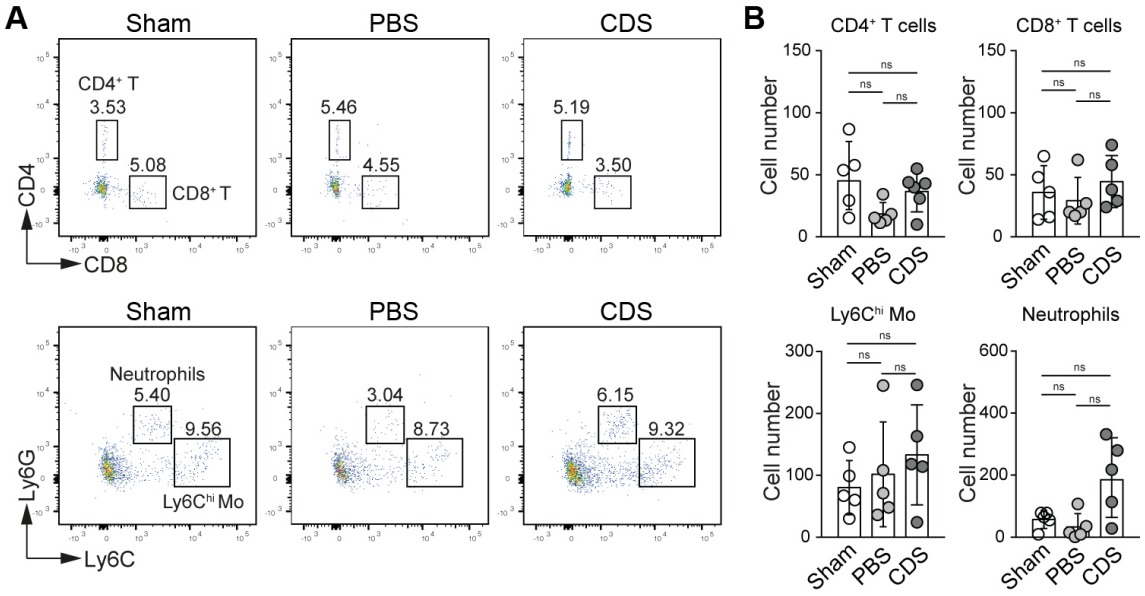

Fig. S5. Number of peripheral immune cells in the PFC of adolescent mice during the peak of microglia depletion relative to controls. To examine whether the stereotaxic surgery causes an infiltration of peripheral immune cells into the PFC, single cell suspensions of prefrontal tissue were prepared at the peak of CDS-induced microglia depletion (i.e., 5 days post-injection; see *Figure 1* in main text) and the numbers of peripheral immune cells in the PFC were quantified using flow cytometry. **(A)** Representative flow cytometry plots of $CD4^+$ and $CD8^+$ T cells (pre-gated on $CD45^{hi}MHCII^-CD11b^-$), neutrophils ($CD45^{hi}CD11b^+Ly6G^+$) and $Ly6C^{hi}$ monocytes (Mo) ($CD45^{hi}CD11b^+Ly6G^{hi}$) in sham controls, PBS controls and CDS mice. **(B)** Number of $CD4^+$ and $CD8^+$ T cells (pre-gated on $CD45^{hi}MHCII^-CD11b^-$), neutrophils ($CD45^{hi}CD11b^+Ly6G^+$) and $Ly6C^{hi}$ monocytes (Mo) ($CD45^{hi}CD11b^+Ly6G^{hi}$) in sham controls, PBS controls and CDS mice. $N = 5$ per group; ns, not significant. The following antibodies were used: anti-mouse MHCII (clone M5/114.15.2), BB700, BD Biosciences, Cat# 746197, RRID:AB_2743544; anti-mouse CD11b (M1/70), BV605, Biolegend, Cat# 101257, RRID:AB_2738811; anti-mouse CD11c (N418), PE-Cy5.5, Thermo Fisher, Cat# 35-0114-82, RRID:AB_10900261; anti-mouse CD45 (30-F11), PE-Cy5,BD Biosciences, Cat# 553082, RRID:AB_2651134; anti-mouse Ly6C (HK1.4), BV711, Biolegend, Cat# 128037, RRID: AB_2562630; anti-mouse Ly6G (1A8), BV650, Biolegend, Cat#127641, RRID:AB_2739334; anti -mouse CD4 (GK1.5), APC, Biolegend, Cat# 100412, RRID:AB_312697; and anti-mouse CD8 (53-6.7), PE-Dazzle, BD Biosciences, Cat# 562283, RRID:AB_11152075.

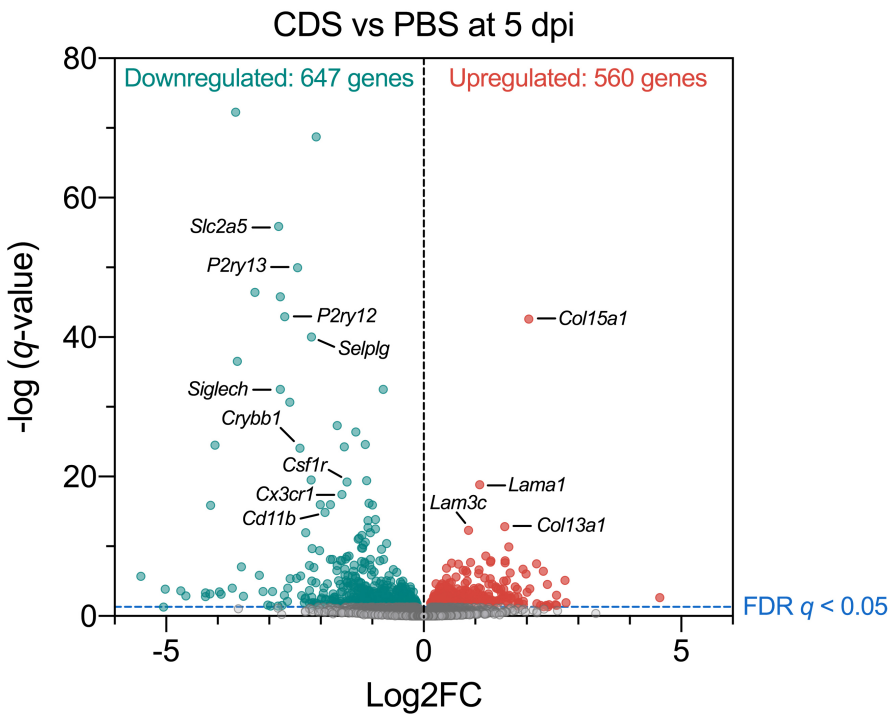

Fig. S6. Differential gene expression in the PFC after PBS or CDS treatment in adolescent mice. The volcano plot depicts the statical significance (-log [*q*-value]) versus the magnitude of gene expression changes (log2 fold change, Log2FC) in the PFC of CDS mice ($N = 5$ males) relative to PBS mice ($N = 5$ males) subjected to next-generation RNA sequencing (RNAseq) at 5 days post-injection (5 dpi). Using a false-discovery rate (FDR) threshold of $q < 0.05$ (indicated by the dashed blue line), 647 genes (green dots) and 560 genes (red dots) were down- and upregulated, respectively, in CDS mice relative to PBS mice. Microglia-defining genes, including *Slc2a5*, *P2ry13*, *P2ry12*, *Selplg*, *Siglech*, *Crybb1, Csf1r*, *Cx3cr1*, and *Cd11b*, were amongst the most strongly downregulated genes in CDS-injected mice. On the other hand, genes pertaining to extracellular matrix remodeling, including *Lama1*, *Lamc3c*, *Col13a1*, and *Col15a1*, were amongst the most strongly upregulated genes in CDS-injected mice.

Microglia-defining genes			
Gene symbol	**Gene ID**	**Log2 FC**	***q*-value**
Cd11b	ENSMUSG00000030786	-1.9155	1.37E-15 *
Csf1r	ENSMUSG00000024621	-1.4916	5.87E-20 *
Cx3cr1	ENSMUSG00000052336	-1.5871	3.69E-18 *
Fcrls	ENSMUSG00000015852	-1.2086	1.41E-08 *
P2ry12	ENSMUSG00000036353	-2.6962	1.23E-43 *
P2ry13	ENSMUSG00000036362	-2.4465	1.09E-50 *
Pu.1	ENSMUSG00000002111	-0.4048	3.04E-01
Selplg	ENSMUSG00000048163	-2.1769	9.89E-41 *
Tmem119	ENSMUSG00000054675	-1.2490	6.67E-12 *
Trem2	ENSMUSG00000023992	-1.3231	1.96E-06 *
Astrocyte-defining genes			
Gene symbol	**Gene ID**	**Log2 FC**	***q*-value**
Acsbg1	ENSMUSG00000032281	-0.0983	6.98E-01
Aldh1l1	ENSMUSG00000030088	0.2103	2.43E-01
Aldoc	ENSMUSG00000017390	-0.0287	9.24E-01
Aqp4	ENSMUSG00000024411	0.1973	3.99E-01
Atp1a2	ENSMUSG00000007097	0.0028	9.90E-01
Papss2	ENSMUSG00000024899	-0.2122	3.88E-01
S100b	ENSMUSG00000033208	0.0053	9.94E-01
Slc1a3	ENSMUSG00000005360	0.0029	9.92E-01
Slc25a18	ENSMUSG00000004902	-0.1586	5.64E-01
Tmem166	ENSMUSG00000035104	-0.0486	9.10E-01
Neuron-defining genes			
Gene symbol	**Gene ID**	**Log2 FC**	***q*-value**
Calb1	ENSMUSG00000028222	-0.1359	5.83E-01
Dlx1	ENSMUSG00000041911	-0.1448	7.43E-01
Htr2c	ENSMUSG00000041380	-0.0793	8.58E-01
Neurod6	ENSMUSG00000037984	0.0771	7.03E-01
Npas4	ENSMUSG00000045903	0.0443	9.57E-01
Pvalb	ENSMUSG00000005716	0.0697	8.88E-01
Slc12a5	ENSMUSG00000017740	0.0802	7.98E-01
Slc17a6	ENSMUSG00000030500	0.0115	9.72E-01
Snap25	ENSMUSG00000027273	0.1553	4.84E-01
Sstr2	ENSMUSG00000047904	0.2177	1.67E-01
Oligodendrocyte-defining genes			
Gene symbol	**Gene ID**	**Log2 FC**	***q*-value**
Cldn11	ENSMUSG00000037625	0.7387	6.60E-02
Mag	ENSMUSG00000036634	0.6517	1.28E-01
Mal	ENSMUSG00000027375	0.5754	5.17E-01

Mbp	ENSMUSG00000041607	0.6600	5.77E-02
Mog	ENSMUSG00000076439	0.4572	3.57E-01
Opalin	ENSMUSG00000050121	0.6548	1.74E-01
Sgk2	ENSMUSG00000017868	0.2978	6.83E-01
Trf	ENSMUSG00000032554	0.2935	5.77E-01
Tspan2	ENSMUSG00000027858	0.4254	1.34E-01
Ugt8a	ENSMUSG00000032854	0.3135	5.35E-01
Endothelial cell-defining genes			
Gene symbol	**Gene ID**	**Log2 FC**	***q*-value**
Abcb1a	ENSMUSG00000040584	0.0004	9.86E-01
Abcb1b	ENSMUSG00000028970	-0.0416	9.20E-01
Apold1	ENSMUSG00000090698	0.0516	9.55E-01
Bsg	ENSMUSG00000023175	0.0782	7.07E-01
Cd34	ENSMUSG00000016494	-0.0504	9.06E-01
Ftl1	ENSMUSG00000050708	0.1848	3.96E-01
Ifitm1	ENSMUSG00000025491	0.0966	8.54E-01
Itm2a	ENSMUSG00000031239	0.1736	3.76E-01
Rgs5	ENSMUSG00000026678	0.0634	7.89E-01
Vwf	ENSMUSG00000001930	0.4147	1.43E-01

Table S1. Summary of gene expression changes characterizing distinct cell populations during the acute phase of prefrontal microglia depletion in adolescence. For each cell population of interest, the table summarizes the magnitude of gene expression changes (log2 fold change, log2FC) in the PFC of CDS mice ($N = 5$) relative to PBS mice ($N = 5$) subjected to next-generation RNA sequencing (RNAseq) at 5 days post-injection. The genes defining microglia, astrocytes, neurons, oligodendrocytes, and vascular endothelial cells were selected based on existing RNAseq databases (*66,68-70*). For each gene of interest, the table also specifies the gene ID and the statistical significance (q-value). Genes that passed a false discovery rate (FDR) correction set at a 5% threshold ($q < 0.05$) were considered as significant and are marked by the symbol (*).

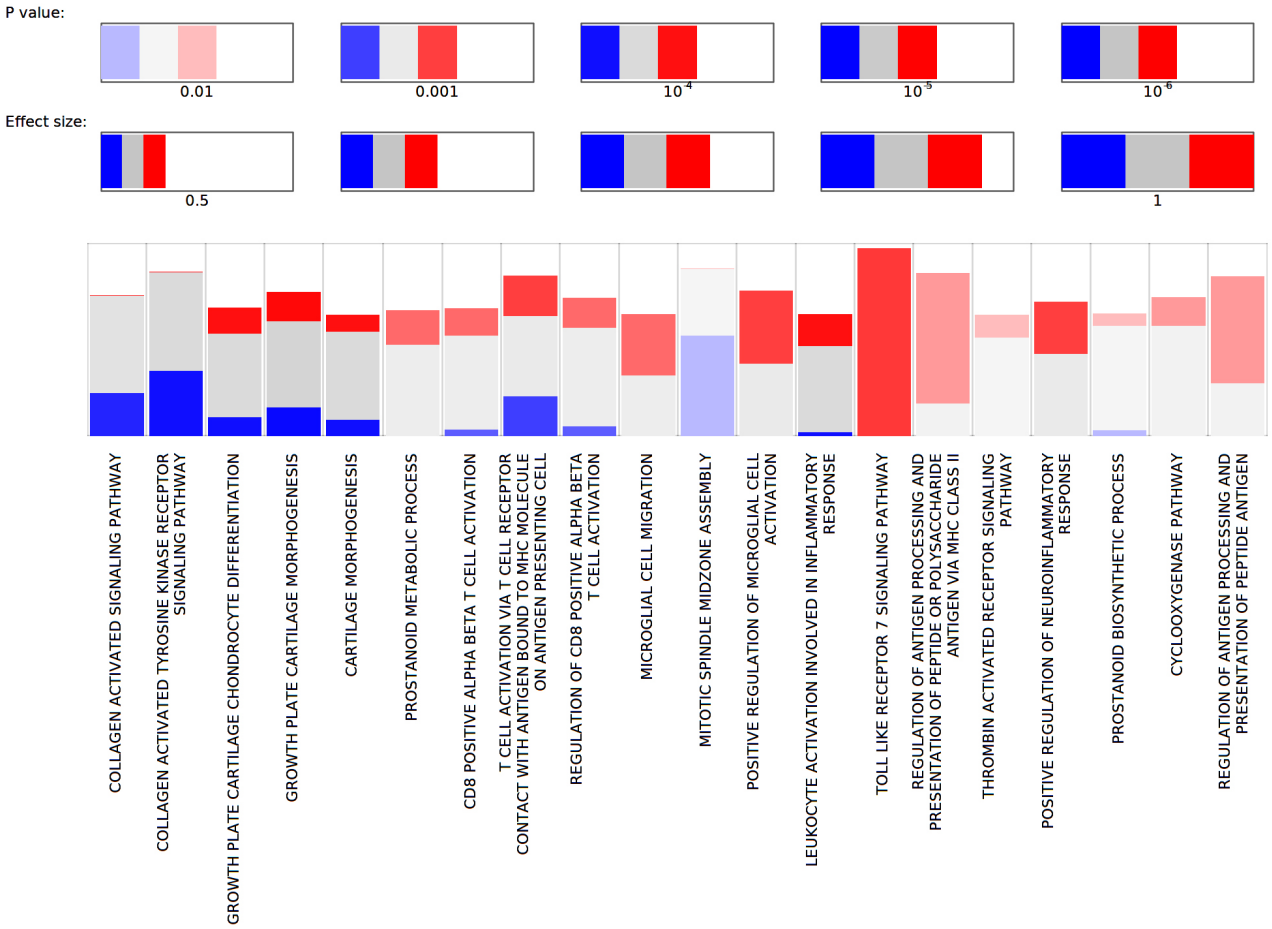

Fig. S7. Transcriptional module (tmod) analysis showing multivariate enrichment results for gene sets revealed by next-generation RNA sequencing after PBS or CDS treatment in adolescent mice. The panel plot depicts gene sets derived from clustering expression profiles that were downregulated (red) and upregulated (blue), respectively, in the PFC of CDS mice ($N = 5$) relative to PBS mice ($N = 5$) at the peak of microglia depletion (i.e. at the 5-days post-injection interval; see *figure S6*). The plot was generated in *R* and represents the gene sets in terms of *p*-values and effect sizes.

Upregulated genes in CDS versus PBS mice at 12 weeks of age			
Gene symbol	**Gene ID**	**Log2 FC**	***q*-value**
Abca8a	ENSMUSG00000041828	0.5731	3.47E-04
Acot11	ENSMUSG00000034853	0.2071	2.41E-02
Col13a1	ENSMUSG00000058806	1.3141	6.20E-09
Col15a1	ENSMUSG00000028339	1.6108	1.65E-24
Col4a6	ENSMUSG00000031273	0.8284	2.67E-02
Cybb	ENSMUSG00000015340	1.4682	3.41E-03
Edn3	ENSMUSG00000027524	0.9567	1.78E-07
Enpp1	ENSMUSG00000037370	0.7824	3.86E-03
Fbln2	ENSMUSG00000064080	0.6448	5.20E-03
Ggt1	ENSMUSG00000006345	0.7254	1.11E-02
H2-Ab1	ENSMUSG00000073421	0.9350	3.43E-02
Itih5	ENSMUSG00000025780	0.5876	2.55E-06
Kif5a	ENSMUSG00000074657	0.2695	3.12E-03
Lama1	ENSMUSG00000032796	0.6873	1.26E-06
Lamc3	ENSMUSG00000026840	0.4983	4.47E-03
Lum	ENSMUSG00000036446	1.3308	1.13E-04
Postn	ENSMUSG00000027750	1.1762	2.11E-02
Spp1	ENSMUSG00000029304	1.6083	3.47E-04
Tbx18	ENSMUSG00000032419	0.7387	1.52E-04
Downregulated genes in CDS versus PBS mice at 12 weeks of age			
Gene symbol	**Gene ID**	**Log2 FC**	***q*-value**
Aldh1a3	ENSMUSG00000015134	-0.9903	1.72E-06
C1ql1	ENSMUSG00000045532	-1.4117	6.67E-17
Cd163	ENSMUSG00000008845	-2.4181	3.15E-20
Cd209b	ENSMUSG00000065987	-2.9444	2.11E-02
Cd209f	ENSMUSG00000051906	-2.5933	4.52E-04
Cspg4	ENSMUSG00000032911	-0.6756	3.47E-04
Gpr17	ENSMUSG00000052229	-0.9199	1.51E-02
Gucy2f	ENSMUSG00000042282	-1.1100	1.37E-03
Inava	ENSMUSG00000041605	-1.0548	1.30E-02
Lad1	ENSMUSG00000041782	-2.1031	6.20E-09
Lhfpl3	ENSMUSG00000106379	-0.4454	4.57E-02
Matn4	ENSMUSG00000016995	-1.4446	1.84E-16
Neu4	ENSMUSG00000034000	-1.5554	1.39E-16
Nrarp	ENSMUSG00000078202	-0.4547	1.71E-02
Olig2	ENSMUSG00000039830	-0.4977	3.86E-03
Pdgfra	ENSMUSG00000029231	-0.8382	5.61E-10
Shc4	ENSMUSG00000035109	-0.5868	2.63E-03
Slc2a5	ENSMUSG00000028976	-0.5609	5.92E-03
Snx22	ENSMUSG00000039452	-1.1169	5.57E-07
Vcan	ENSMUSG00000021614	-0.6023	3.27E-02

Table S2 *(previous page)*. Differential gene expression in the adult PFC after PBS or CDS treatment in adolescence. The table summarizes the differentially expressed genes (DEG) in the PFC of adult (12-week-old) mice treated with CDS in adolescence (6 weeks of age; see *fig. S1*) relative to adult mice treated with PBS in adolescence (N = 5 per group). Differential gene expression of next-generation RNA sequencing (RNAseq) data was obtained using a false-discovery rate (FDR) threshold of $q < 0.05$. Using this FDR, 20 and 19 genes were down- and upregulated, respectively, in CDS mice relative to PBS mice. For each DEG, the table specifies the gene symbol, gene ID, magnitude of gene expression changes (log2 fold change, log2FC), and statical significance (q-value).

Microglia-defining genes			
Gene symbol	**Gene ID**	**Log2 FC**	***q*-value**
Cd11b	ENSMUSG00000030786	-0.3419	1.00E+00
Csf1r	ENSMUSG00000024621	-0.4581	4.96E-01
Cx3cr1	ENSMUSG00000052336	-0.4740	6.84E-01
Fcrls	ENSMUSG00000015852	0.0127	1.00E+00
P2ry12	ENSMUSG00000036353	-0.3971	1.00E+00
P2ry13	ENSMUSG00000036362	-0.4439	5.53E-01
Pu.1	ENSMUSG00000002111	-0.3632	1.00E+00
Selplg	ENSMUSG00000048163	-0.5252	2.02E-01
Tmem119	ENSMUSG00000054675	-0.3365	1.00E+00
Trem2	ENSMUSG00000023992	-0.2495	1.00E+00
Astrocyte-defining genes			
Gene symbol	**Gene ID**	**Log2 FC**	***q*-value**
Acsbg1	ENSMUSG00000032281	0.1326	1.00E+00
Aldh1l1	ENSMUSG00000030088	0.1468	1.00E+00
Aldoc	ENSMUSG00000017390	0.1084	1.00E+00
Aqp4	ENSMUSG00000024411	0.0318	1.00E+00
Atp1a2	ENSMUSG00000007097	0.1041	1.00E+00
Papss2	ENSMUSG00000024899	-0.1927	1.00E+00
S100b	ENSMUSG00000033208	0.1169	1.00E+00
Slc1a3	ENSMUSG00000005360	0.0119	1.00E+00
Slc25a18	ENSMUSG00000004902	0.1332	1.00E+00
Tmem166	ENSMUSG00000035104	0.0346	1.00E+00
Neuron-defining genes			
Gene symbol	**Gene ID**	**Log2 FC**	***q*-value**
Calb1	ENSMUSG00000028222	-0.0388	1.00E+00
Dlx1	ENSMUSG00000041911	0.1288	1.00E+00
Htr2c	ENSMUSG00000041380	-0.1752	1.00E+00
Neurod6	ENSMUSG00000037984	-0.0228	1.00E+00
Npas4	ENSMUSG00000045903	-0.3065	1.00E+00
Pvalb	ENSMUSG00000005716	0.3024	1.00E+00
Slc12a5	ENSMUSG00000017740	-0.0157	1.00E+00
Slc17a6	ENSMUSG00000030500	-0.1401	1.00E+00
Snap25	ENSMUSG00000027273	0.0014	1.00E+00
Sstr2	ENSMUSG00000047904	0.0220	1.00E+00
Oligodendrocyte-defining genes			
Gene symbol	**Gene ID**	**Log2 FC**	***q*-value**
Cldn11	ENSMUSG00000037625	0.4467	1.00E+00
Mag	ENSMUSG00000036634	0.4207	1.00E+00
Mal	ENSMUSG00000027375	0.5283	1.00E+00

Mbp	ENSMUSG00000041607	0.4952	1.00E+00
Mog	ENSMUSG00000076439	0.4297	1.00E+00
Opalin	ENSMUSG00000050121	0.3610	1.00E+00
Sgk2	ENSMUSG00000017868	0.0533	1.00E+00
Trf	ENSMUSG00000032554	0.6431	9.24E-01
Tspan2	ENSMUSG00000027858	0.1863	1.00E+00
Ugt8a	ENSMUSG00000032854	0.4391	1.00E+00
Endothelial cell-defining genes			
Gene symbol	**Gene ID**	**Log2 FC**	***q*-value**
Abcb1a	ENSMUSG00000040584	0.0540	1.00E+00
Abcb1b	ENSMUSG00000028970	0.0571	1.00E+00
Apold1	ENSMUSG00000090698	0.3277	1.00E+00
Bsg	ENSMUSG00000023175	0.0618	1.00E+00
Cd34	ENSMUSG00000016494	0.1422	1.00E+00
Ftl1	ENSMUSG00000050708	0.0898	1.00E+00
Ifitm1	ENSMUSG00000025491	-0.3135	1.00E+00
Itm2a	ENSMUSG00000031239	-0.0804	1.00E+00
Rgs5	ENSMUSG00000026678	0.1239	1.00E+00
Vwf	ENSMUSG00000001930	0.0205	1.00E+00

Table S3. Summary of gene expression characterizing distinct cell populations in the adult PFC after PBS or CDS treatment in adolescence. For each cell population of interest, the table summarizes the magnitude of gene expression (log2 fold change, log2FC) in the PFC of adult (12-week-old) mice treated with CDS in adolescence (6 weeks of age; see *fig. S1*) relative to adult mice treated with PBS in adolescence. Differential gene expression of next-generation RNA sequencing (RNAseq) data was obtained using a false-discovery rate (FDR) threshold of $q < 0.05$. The genes defining microglia, astrocytes, neurons, oligodendrocytes, and vascular endothelial cells were selected based on existing RNAseq databases (*66,68-70*). For each gene of interest, the table also specifies the gene ID and the statistical significance (q-value). Genes that passed a false discovery rate (FDR) correction set at a 5% threshold ($q < 0.05$) were considered as significant.

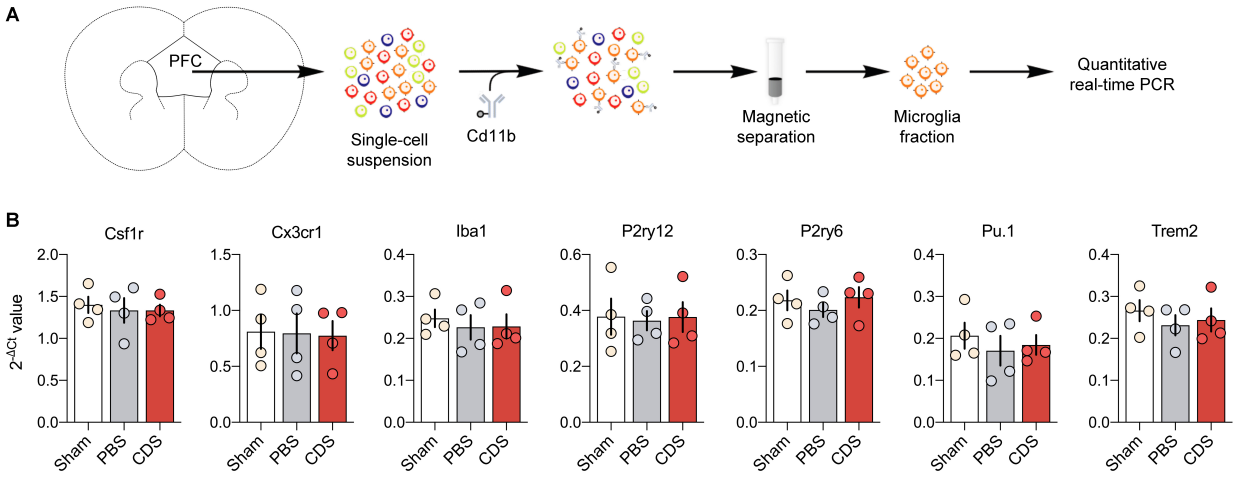

Fig. S8. Quantification of microglia-defining genes in microglia isolated from the PFC of adult mice subjected to sham, PBS or CDS treatment in adolescence. Microglia-defining genes were analyzed in microglia isolated from the PFC of adult (12 weeks of age) male mice that received an intracerebral CDS or PBS injection into the PFC or were sham-operated during adolescence (see *figure S1*). **(A)** Principal experimental design used to isolate microglia from the PFC using magnetic-activated cell sorting (MACS). Single-cell suspensions generated from PFC samples were incubated with anti-CD11b magnetic microbeads to obtain a microglial cell fraction through positive magnetic selection. The microglial cell fraction was then used to quantify the expression of microglia-defining genes by means of quantitative real-time polymerase chain reaction (qRT-PCR). **(B)** The bar plots show mRNA levels of Csf1r, Cx3cr1, Iba1 (= Aif1), P2ry12, P2ry6, Pu.1 (= Spi1) and Trem2 in prefrontal microglia of adult sham, PBS and CDS mice. Each data point corresponds to pooled PFC samples from 3 male mice, with independent 4 replicates per group. All data are means ± SEM with individual values overlaid.

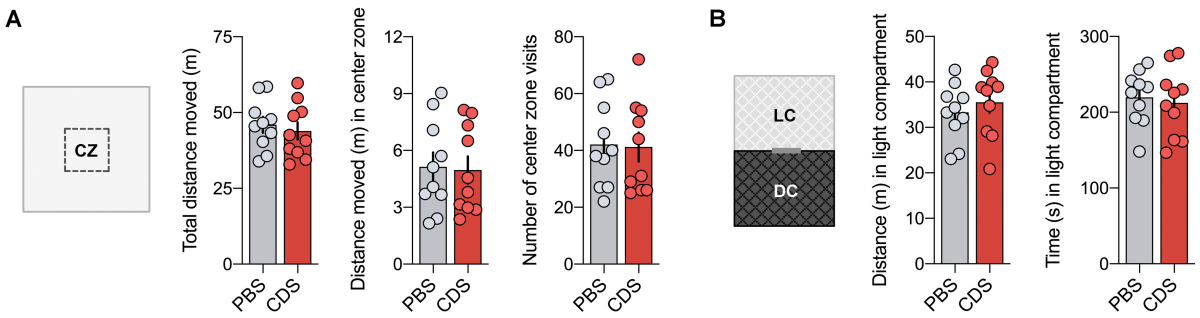

Fig. S9. Basal locomotor activity and anxiety-related behavior in adult mice subjected to PBS or CDS treatment in adolescence. Male mice that received either a CDS or PBS injection during adolescence (see *figure S1*) and were subjected to behavioral testing once they reached adulthood (12 weeks onwards). **(A)** Total distance moved, distance moved in the center zone (CZ) and number of CZ visits in PBS and CDS mice during the open field test. **(B)** Distance moved and time spent in the light compartment (LC) in PBS and CDS mice during the light-dark box test, which measures the animals' exploration of the LC relative to the dark compartment (DC). All data are means ± SEM with individual values overlaid; $N = 10$ mice per group and test.

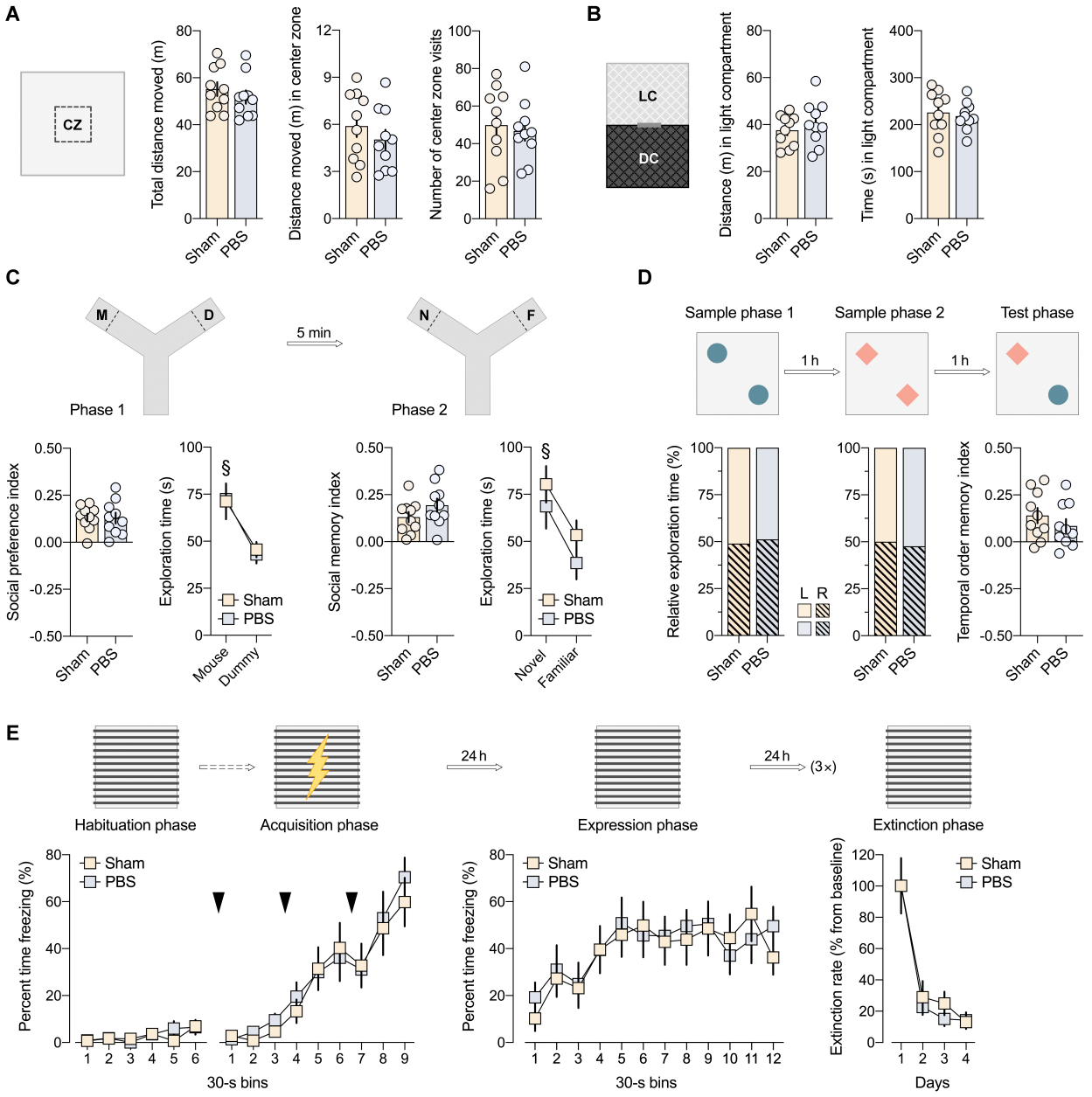

Fig. S10. Behavioral and cognitive performance of adult mice subjected to sham operation or intracerebral PBS injection in adolescence. Male mice receiving no stereotaxic injection (sham control mice) were compared to mice receiving a bilateral stereotaxic injection of PBS in adolescence (see *figure S1*) using a battery of behavioral and cognitive tests in adulthood. **(A)** Total distance moved, distance moved in the center zone (CZ) and number of CZ visits during the open field test. **(B)** Distance moved and time spent in the light compartment (LC) during the light-dark box test, which measures the animals' exploration of the LC relative to the dark compartment (DC). **(C)** Phase 1 (D = dummy object, M = unfamiliar mouse) and phase 2 (F = familiar mouse; N = novel mouse) of the social interaction test. The bar plots show the

social preference index in phase 1 (values > 0 represent a preference towards M) and social memory index in phase 2 (values > 0 represent a preference towards N), whereas the line plots depict absolute exploration times in either phase. $^{\S}p < 0.001$, reflecting the overall main effect of object in phase 1 ($F_{(1,18)} = 36.7$) and phase 2 ($F_{(1,18)} = 22.3$) **(D)** The percentage bar plots depict the relative amount of time (%) exploring the left (L) or right (R) object in sample phase 1 and 2 of the temporal order memory test. The bar plot shows the temporal order memory index during the test phase (values > 0 represent a preference towards the temporally more remote object presented in sample phase 1). **(E)** Acquisition, expression and extinction of contextual fear. The line plots show percent time freezing during the habituation, acquisition and expression phases, as well as the extinction rate (% change from freezing levels measured during the expression phase). The arrows indicate the presentation of a mild electric foot shock. All data are means ± SEM with individual values overlaid; *N*(sham) = 10 mice, *N*(PBS) = 10 mice for each test.

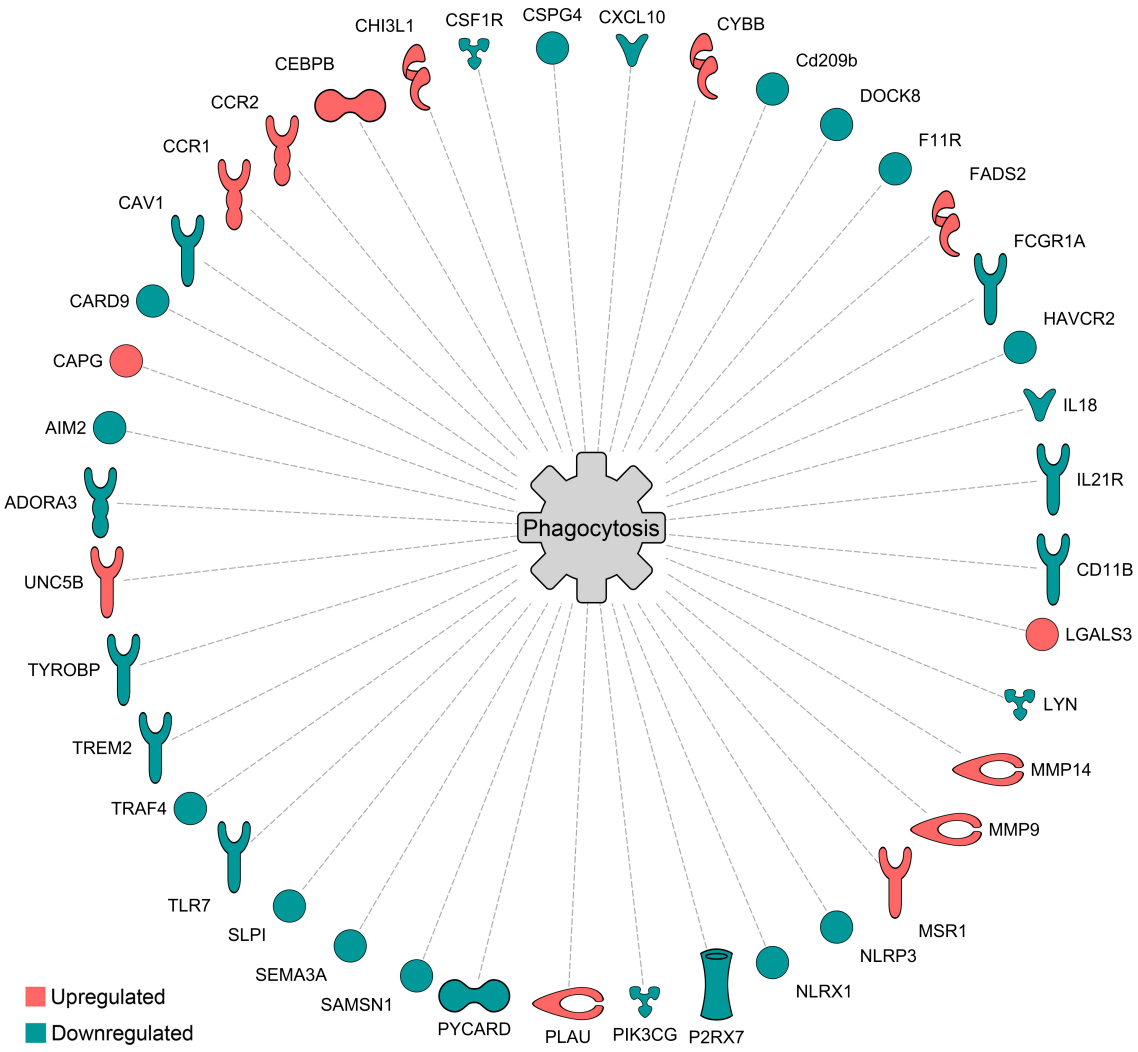

Fig. S11. Graphical representation of differentially expressed genes annotated with the functional network "phagocytosis" during the acute phase of adolescent microglia depletion. Ingenuity pathway analysis (IPA) was used for functional network prediction of genes that were found to be differentially expressed in the PFC of mice subjected to CDS ($N = 5$) or PBS ($N = 5$) treatment in adolescence (6 weeks of age; see *figure S1*). Next-generation RNA sequencing (RNAseq) was conducted during the acute phase of CDS-induced microglia depletion (i.e., at 5 days post-injection) and analyzed using a false discovery rate (FDR) correction set at a 5% threshold ($q < 0.05$; see *figure S6*). IPA identified the functional network "phagocytosis" to be dysregulated during the acute phase of adolescent microglia depletion. Genes that were upregulated in CDS relative to PBS mice are shown in red; genes that were downregulated in CDS relative to PBS mice are shown in green.

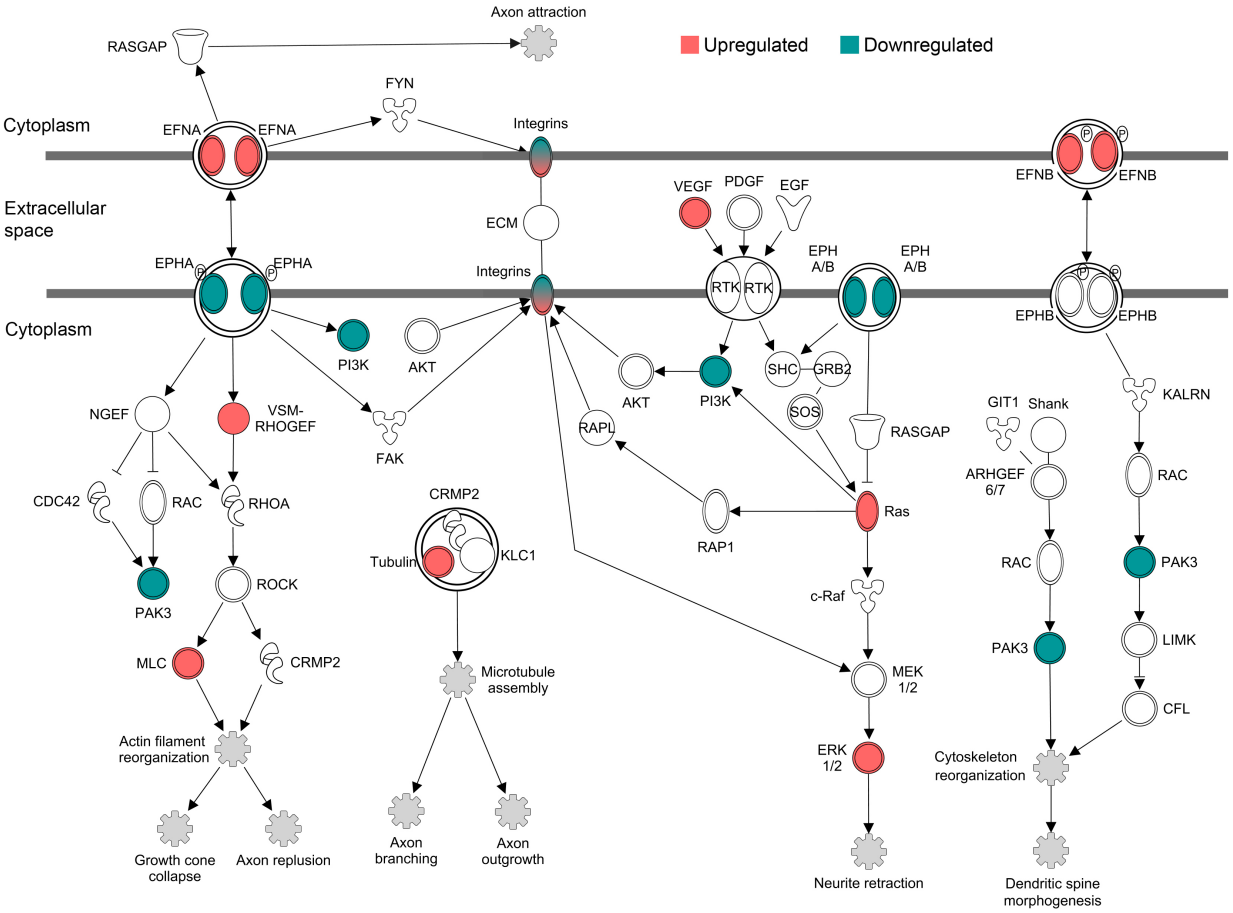

Fig. S12. Graphical representation of differentially expressed genes annotated with the functional networks "axonal remodeling", "neurite remodeling" and "dendritic spine morphogenesis" during the acute phase of adolescent microglia depletion. Ingenuity pathway analysis (IPA) was used for functional network prediction of genes that were found to be differentially expressed in the PFC of mice subjected to CDS (N = 5) or PBS (N= 5) treatment in adolescence (6 weeks of age; see *figure S1*). Next-generation RNA sequencing (RNAseq) was conducted during the acute phase of CDS-induced microglia depletion (i.e., at 5 days post-injection) and analyzed using a false discovery rate (FDR) correction set at a 5% threshold ($q < 0.05$; see *figure S6*). IPA identified the functional networks "axonal remodeling", "neurite remodeling" and "dendritic spine morphogenesis" to be dysregulated during the acute phase of adolescent microglia depletion. Genes that were upregulated in CDS relative to PBS mice are shown in red; genes that were downregulated in CDS relative to PBS mice are shown in green.

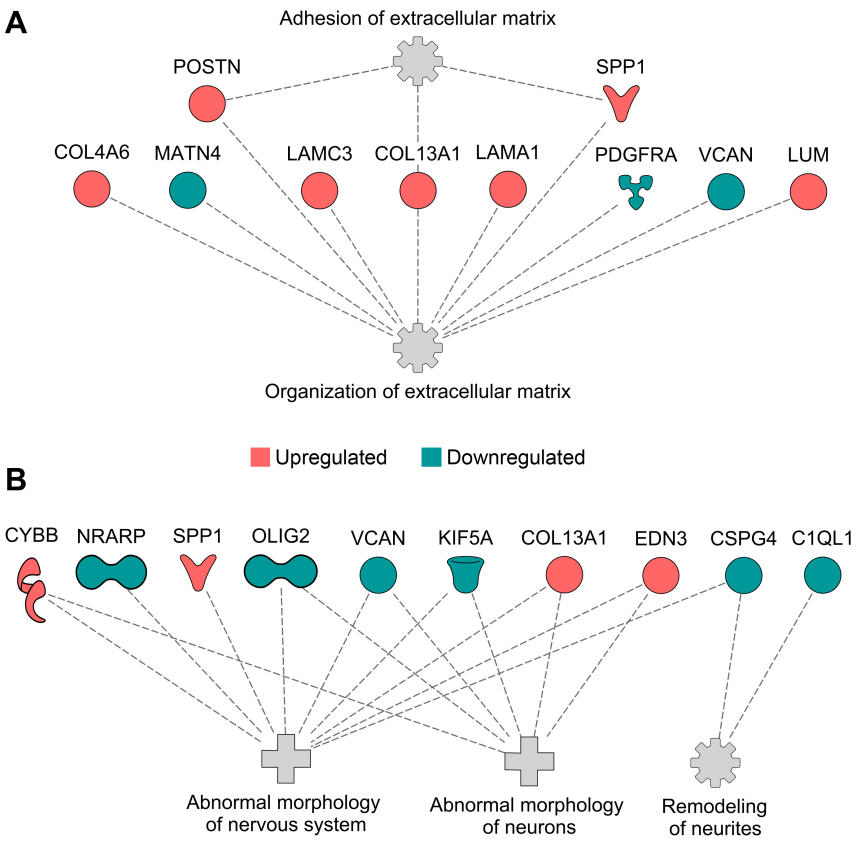

Fig. S13. Graphical representation of differentially expressed genes annotated with the functional networks "extracellular matrix organization and functions", "abnormal morphology of nervous system", "abnormal morphology of neurons", and "remodeling of neurites" in the PFC of adult mice subjected to PBS or CDS treatment in adolescence. Ingenuity pathway analysis (IPA) was used for functional network prediction of genes that were found to be differentially expressed in the PFC of adult mice subjected to CDS ($N = 5$) relative to PBS ($N = 5$) treatment in adolescence (6 weeks of age; see *figure S1*). Next-generation RNA sequencing (RNAseq) was conducted when the animals reached 12 weeks of age and was analyzed using a false discovery rate (FDR) correction set at a 5% threshold ($q < 0.05$; see *Table S2*). Genes that were upregulated in CDS relative to PBS mice are shown in red; genes that were downregulated in CDS relative to PBS mice are shown in green. **(A)** Differentially expressed genes annotated with the functional network "extracellular matrix organization and functions". **(B)** Differentially expressed genes annotated with the functional networks abnormal morphology of nervous system" and "abnormal morphology of neurons", and "remodeling of neurites".

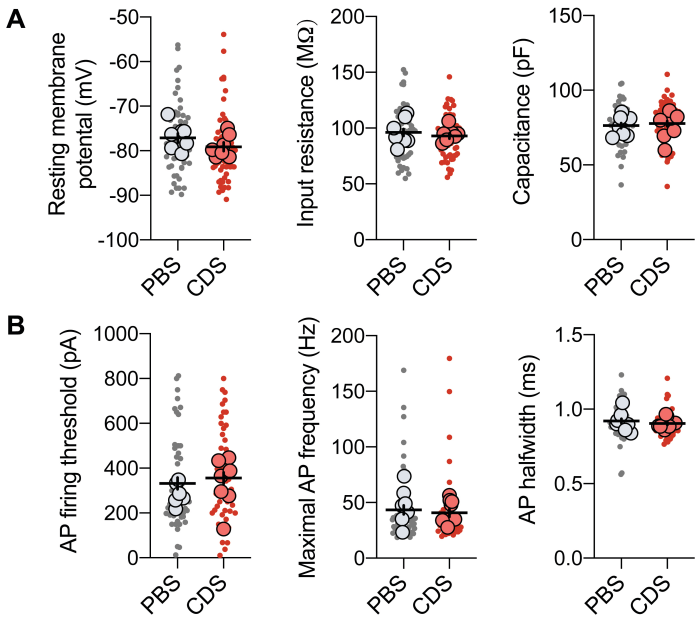

Fig. S14. Transient microglia depletion in the adolescent PFC does not alter main biophysical properties of prefrontal pyramidal neurons in adulthood. To test the effects of adolescent microglia depletion on main biophysical properties of prefrontal pyramidal neurons in adulthood, 6-week-old C57BL6/N male mice received a single, bilateral stereotaxic injection of CDS or PBS into the PFC and were then allowed to recover and mature into adulthood (see *figure S1*). Electrophysiological recordings were conducted when the animals reached 12 weeks of age. **(A)** The scatter plots show measures of passive biophysical properties (resting membrane potential, input resistance and capacitance) in PBS and CDS mice. **(B)** The scatter plots depict measures of action potential (AP)-related properties (AP firing threshold and maximal AP frequency, AP half-width) in PBS and CDS mice. For all data**,** dots represent individual cells (n = 51 for PBS, n = 53 for CDS), whereas filled circles reflect cell averages per animal (N = 7 per group).

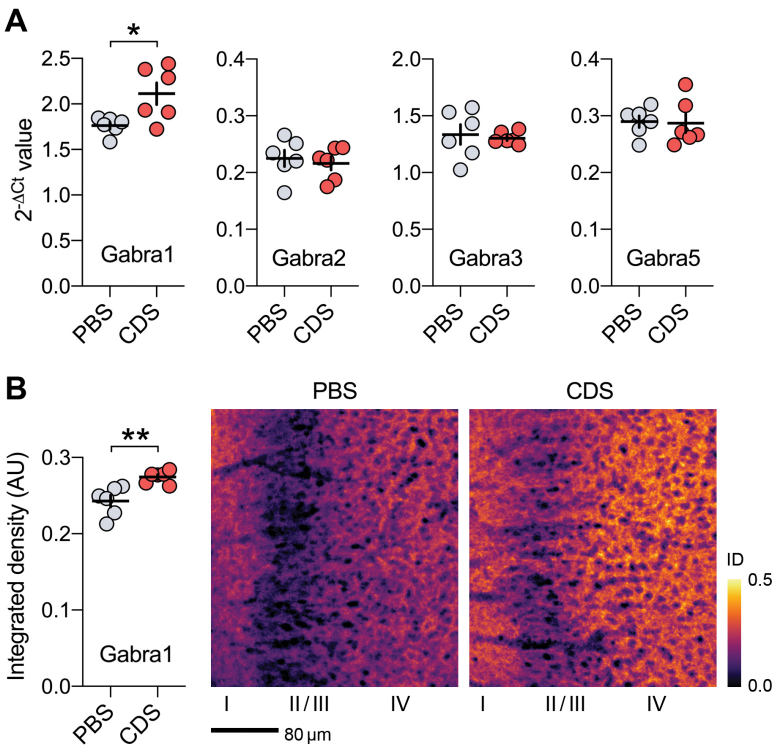

Fig. S15. Selective alterations in GABAergic receptor expression in the adult PFC after transient prefrontal microglia depletion in adolescence. To test the effects of transient prefrontal microglia depletion in adolescence on the expression of GABAergic receptor subunits in the adult PFC, 6-week-old C57BL6/N male mice received a single, bilateral stereotaxic injection of CDS or PBS into the PFC and were then allowed to recover and mature into adulthood (see *figure S1*). **(A)** Quantitative real-time polymerase chain reaction (qRT-PCR) analyses of Gabra1, Gabra2, Gabra3, and Gabra5 mRNA levels in the PFC of adult PBS and CDS mice. $*p < 0.05$, $t_{(10)} = 2.40$; $N = 6$ per group. **(B)** Integrated density (arbitrary units, AU) of Gabra1 protein assessed in the adult PFC of PBS and CDS mice by immunohistochemistry. $**p < 0.01$, $t_{(10)} = 3.70$; $N = 6$ per group. The photomicrographs depict color-coded immunofluorescence stains of Gabra1 immunoreactivity in layers I-IV of the PFC from adult PBS and CDS mice. Strong staining intensities (color-coded integrated densities, ID) appear in orange/yellow.

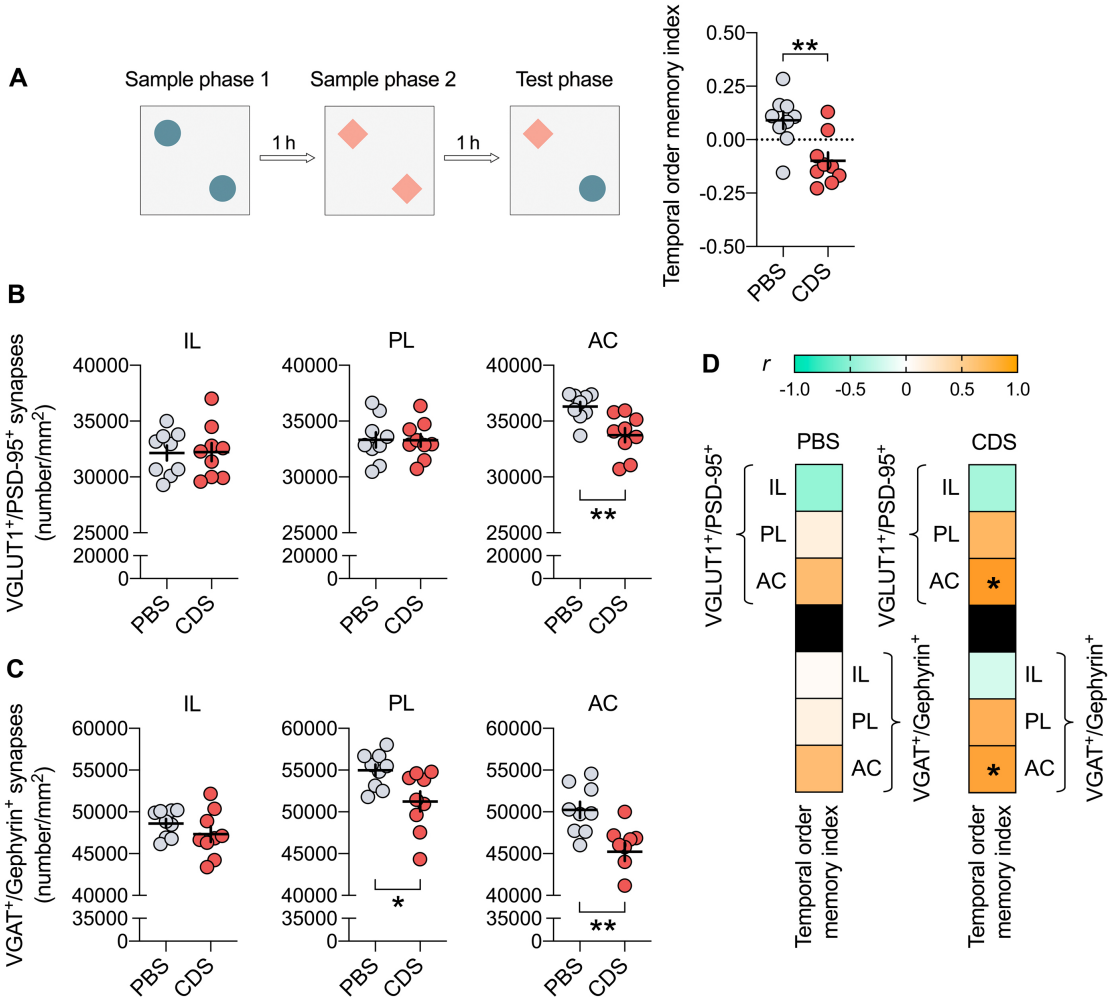

Fig. S16. Relationship between cognitive and subregion-specific synaptic deficits in adult mice after prefrontal microglia deficiency in adolescence. (A) A temporal order memory test was used to confirm the presence of cognitive deficits in an independent cohort of adult mice subjected to transient prefrontal microglia deficiency in adolescence. The scatter plot shows the temporal order memory index for PBS and CDS mice during the test phase. $^{**}p < 0.01$ ($t_{(16)} = 3.40$). $N = 9$ mice per group. **(B)** The scatter plots display the density (number/mm^2) of VGLUT1$^+$/PSD-95$^+$ excitatory synapses in infralimbic (IL), prelimbic (PL) and anterior cingulate (AC) subregions of the PFC from PBS and CDS mice that were subjected to the temporal order memory test previously. $^{**}p < 0.01$, $t_{(16)} = 3.41$. $N = 9$ mice per group. **(C)** The scatter plots show the density (number/mm^2) of VGAT$^+$/Gephyrin$^+$ inhibitory synapses in IL, PL and AC subregions of the PFC from PBS and CDS mice that were subjected to the temporal order memory test previously. $^{*}p < 0.05$ ($t_{(16)} = 2.68$) and $^{*}p < 0.01$ ($t_{(16)} = 3.44$); $N = 9$ mice per group. **(D)** Group-wise Pearson product-moment correlations between the temporal order memory index and the density of excitatory (VGLUT1$^+$/PSD-95$^+$) or inhibitory (VGAT$^+$/Gephyrin$^+$) synapses in different subregions of the PFC from PBS and CDS mice. Positive and negative correlations are represented in orange turquoise color,

respectively. Significant correlations are denoted with the symbol (*) and were corrected for multiple comparisons (significance threshold: $p < 0.0084$; $N = 9$ mice per group). Group-spanning correlations are provided in *fig. S17*.

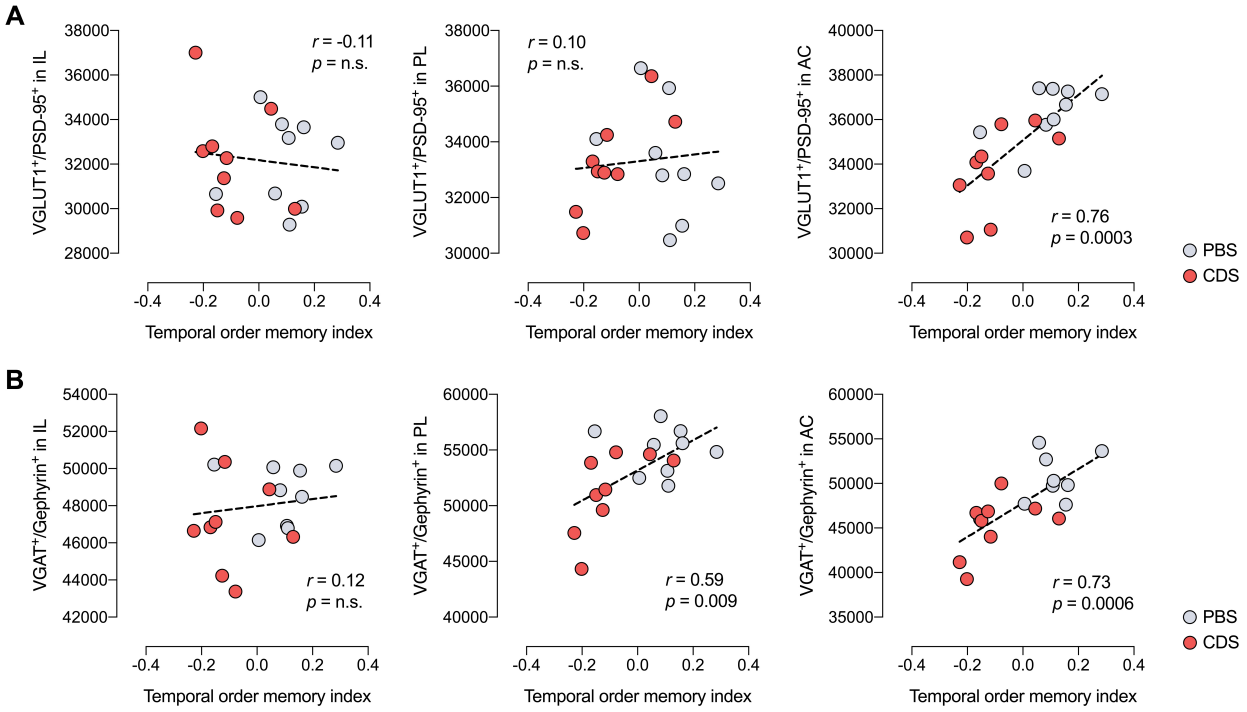

Fig. S17. Group-spanning Pearson product-moment correlations between the temporal order memory index and the density of excitatory (VGLUT1$^+$/PSD-95$^+$) or inhibitory (VGAT$^+$/Gephyrin$^+$) synapses in different subregions of the PFC from PBS and CDS mice. The scatter plots show group-spanning correlations for infralimbic (IL), prelimbic (PL) and anterior cingulate (AC) subregions of the PFC and provide the *p*-values and Pearson correlation coefficient (*r*) for each correlation. **(A)** Correlations between the temporal order memory index and the density of excitatory (VGLUT1$^+$/PSD-95$^+$) synapses in different subregions of the PFC. **(B)** Correlations between the temporal order memory index and the density of inhibitory (VGAT$^+$/Gephyrin$^+$) synapses in different subregions of the PFC. $N = 18$ (9 PBS and 9 CDS) mice; n.s., not significant. Group-wise correlations Pearson product-moment correlations are provided in *Figure 5* of the main document.

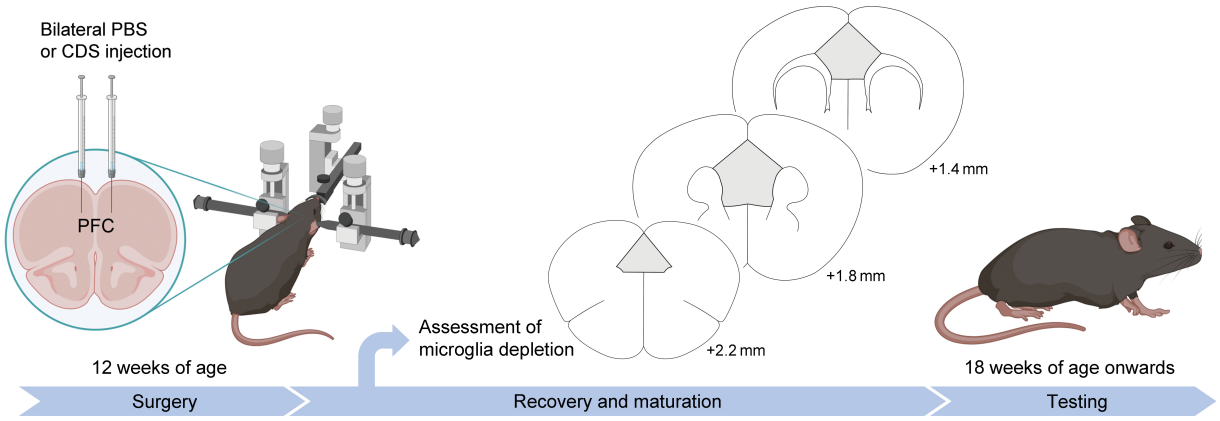

Fig. S18. Experimental design used to investigate the effects of transient microglia depletion in adulthood. To deplete microglia selectively and transiently from the prefrontal cortex in adulthood, 12-week-old C57BL6/N male mice received a single, bilateral stereotaxic injection of CDS into the PFC. Control mice received a bilateral stereotaxic injection of PBS. The magnitude and specificity of microglia depletion was ascertained by post-mortem immunohistochemistry in the PFC (as highlighted by the gray area in the schematic coronal sections) at 5 and 20 days post-injection (dpi) along the anterior (bregma +2.2. mm) to posterior (bregma +1.4 mm) axis. The 5 dpi interval was selected to capture the peak of CDS-induced microglia depletion, whereas the 20 dpi interval was chosen to ascertain the fully restored density of prefrontal microglia after transient depletion in adulthood. To examine possible effects of adult microglia depletion on behavioral and cognitive functions, 12-week-old C57BL6/N male mice were injected with either CDS or PBS and were allowed to recover for 6 weeks. A recovery period of 6 weeks was chosen to match the recovery and maturation period used in experiments, in which microglia were transiently depleted from the PFC of adolescent mice (see *figure S1*). Hence, in the experimental setting of adult microglia depletion, behavioral and cognitive testing commenced at 18 weeks of age.

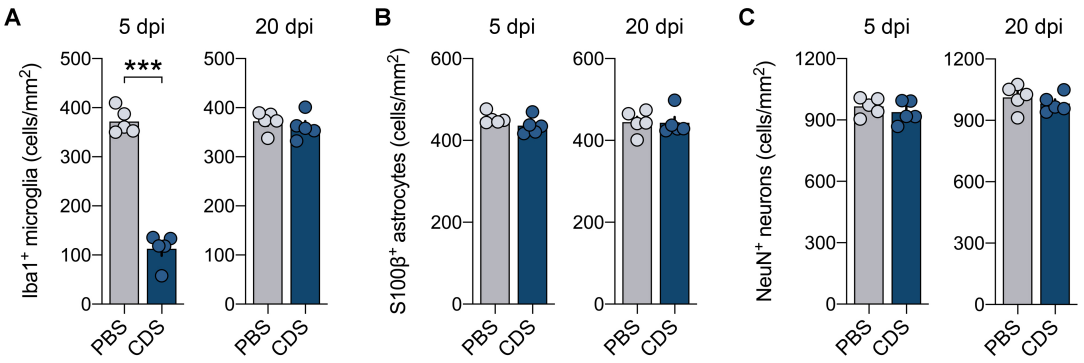

Fig. S19. Density of microglia, neurons and astrocytes in the PFC after PBS or CDS treatment in adulthood. Post-mortem immunohistochemistry was used to assess whether bilateral stereotaxic injection of CDS into the PFC of adult mice alters the density of microglia, neurons and astrocytes at 5 and 20 days post-injection (dpi). **(A)** Number of Iba1$^+$ microglia in the PFC of adult PBS and CDS mice at 5 and 20 dpi. ***$p < 0.001$ ($t_{(8)} = 14.2$). **(B)** Number of S100β$^+$ astrocytes in the PFC of adult PBS and CDS mice at 5 and 20 dpi. **(C)** Number of NeuN$^+$ neurons in the PFC of adult PBS and CDS mice at 5 and 20 dpi. All data are means ± SEM with individual values overlaid; $N = 5$ mice per group and dpi.

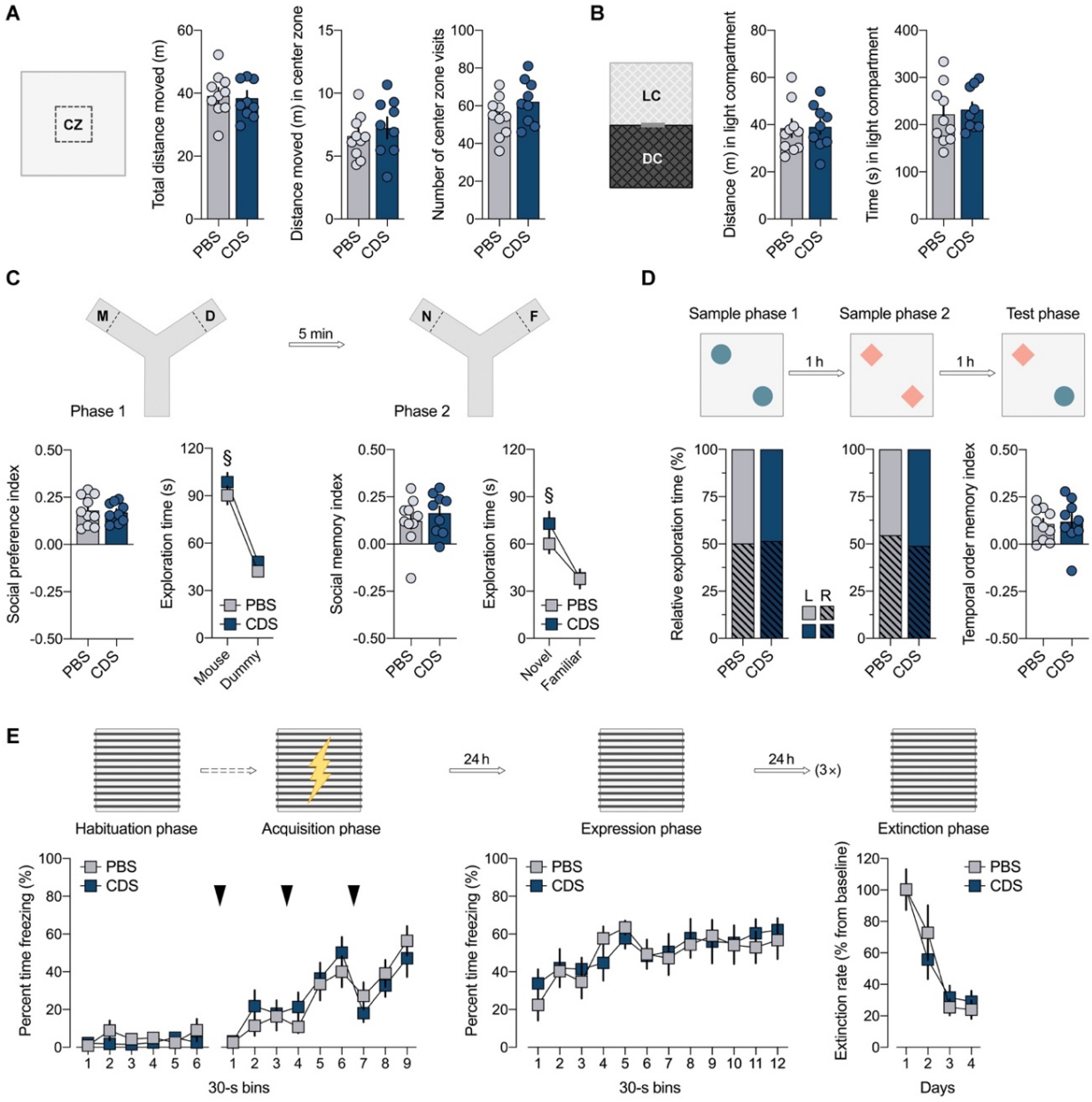

Fig. S20. Transient microglia depletion in the adult PFC does not cause long-term behavioral and cognitive changes. To examine possible effects of prefrontal microglia depletion in adulthood on behavioral and cognitive functions, 12-weeks-old C57BL6/N mice were injected with either CDS or PBS and were allowed to recover for 6 weeks. Behavioral and cognitive testing commenced when the animals reached 18 weeks of age (see *figure S18*). **(A)** Total distance moved, distance moved in the center zone (CZ) and number of CZ visits during the open field test. **(B)** Distance moved and time spent in the light compartment (LC) during the light-dark box test, which measures the animals' exploration of the LC relative to the dark compartment (DC). **(C)** Phase 1 (D = dummy object, M = unfamiliar mouse) and phase 2 (F = familiar mouse; N = novel mouse) of the social interaction test. The bar plots show the social

preference index in phase 1 (values > 0 represent a preference towards M) and social memory index in phase 2 (values > 0 represent a preference towards N), whereas the line plots depict absolute exploration times in either phase. $^{\S}p < 0.001$, reflecting the overall main effect of object in phase 1 ($F_{(1,17)} = 108.8$) and phase 2 ($F_{(1,17)} = 22.7$) **(D)** The percentage bar plots depict the relative amount of time (%) exploring the left (L) or right (R) object in sample phase 1 and 2 of the temporal order memory test. The bar plot shows the temporal order memory index during the test phase (values > 0 represent a preference towards the temporally more remote object presented in sample phase 1). **(E)** Acquisition, expression and extinction of contextual fear. The line plots show percent time freezing during the habituation, acquisition and expression phases, as well as the extinction rate (% change from freezing levels measured during the expression phase). The arrows indicate the presentation of a mild electric foot shock. All data are means ± SEM with individual values overlaid; *N*(PBS) = 10 mice, *N*(CDS) = 9 mice for each test.

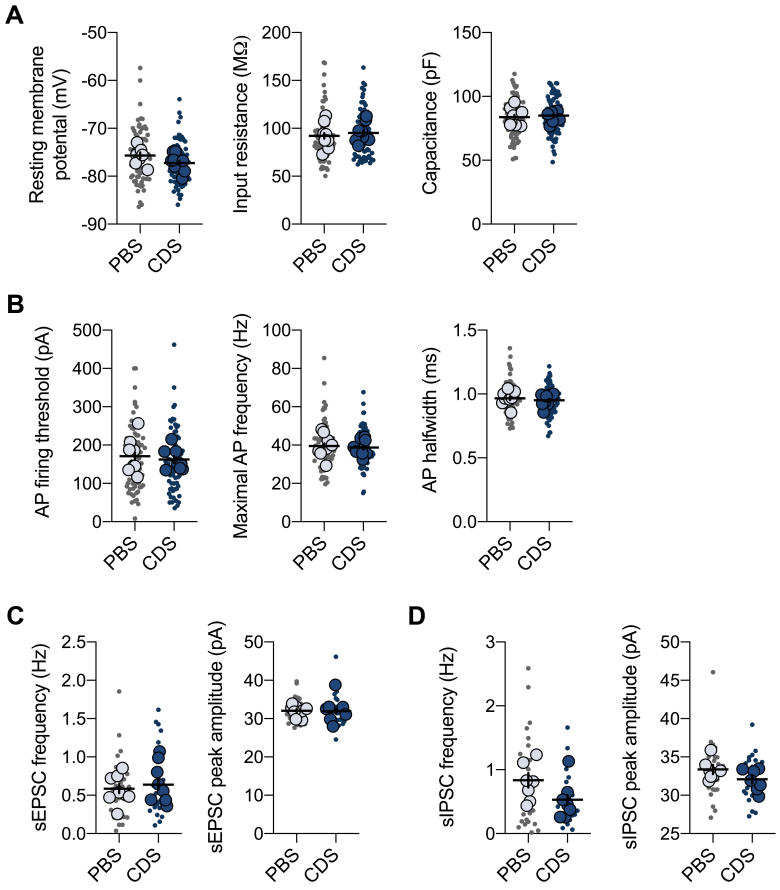

Fig. S21. Electrophysiological parameters of prefrontal pyramidal neurons after transient prefrontal microglia depletion in adulthood. To examine possible effects of transient prefrontal microglia depletion in adulthood on electrophysiological parameters of pyramidal neurons in adulthood, 12-week-old C57BL6/N male mice received a single, bilateral stereotaxic injection of CDS or PBS into the PFC and were then allowed to recover for 6 weeks (see *figure S18*). Electrophysiological recordings were conducted when the animals reached 18 weeks of age. **(A)** Passive biophysical properties (resting membrane potential, input resistance and capacitance) in PBS and CDS mice. Dots represent individual cells (*n*[PBS]= 69 cells and *n*[CDS]= 73 cells; from *N* = 8 mice in each group), whereas filled circles reflect cell averages per animal. **(B)** Action potential (AP)-related properties (AP firing threshold and maximal AP frequency, AP half-width) in PBS and CDS mice. Dots represent individual cells *n*[PBS]= 69 cells and *n*[CDS]= 73 cells; from *N* = 8 mice in each group), whereas filled circles reflect cell averages per animal. **(C)** sEPSC frequency and peak amplitude of pyramidal neurons in the PFC of PBS and CDS mice. Dots represent individual cells (*n*[PBS]= 29 cells and *n*[CDS]= 28 cells; from *N* = 8 mice in each group), whereas filled circles reflect cell averages per animal. **(D)** sIPSC frequency and peak amplitude of pyramidal neurons in the PFC of PBS and CDS mice. Dots represent individual cells (*n*[PBS]= 26 cells and *n*[CDS]= 20 cells; from *N* = 7 mice in each group), whereas filled circles reflect cell averages per animal.

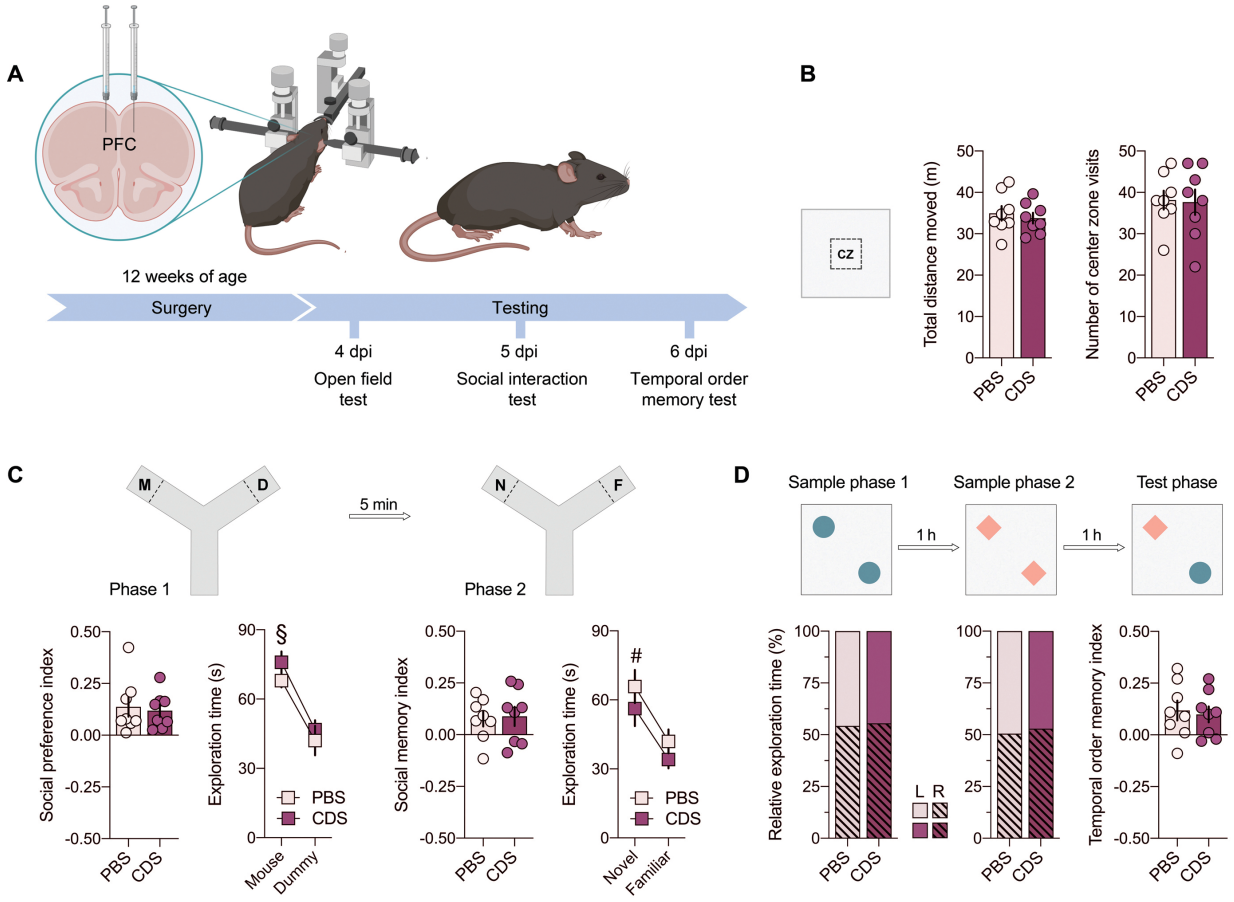

Fig. S22. Microglia depletion in the adult PFC does not cause behavioral and cognitive changes during the acute phase of depletion. (A) Experimental design used to test whether CDS-induced microglia depletion in the adult PFC induces behavioral and cognitive changes during the acute phase of depletion. 12-week-old male C57BL6/N mice received a single, bilateral stereotaxic injection of CDS into the PFC. Control mice received a bilateral stereotaxic injection of PBS. To assess possible changes in behavior and cognition during the acute phase of prefrontal microglia depletion, PBS and CDS mice were tested at 4 days post-injection (4 dpi; open field test), 5 dpi (social interaction test) and 6 dpi (temporal order memory test). These dpi intervals were selected because they correspond to the peak of microglia depletion after intra-PFC injection of CDS (see *Fig. 1* in main document and *fig. S19A* in Supplement). **(B)** Total distance moved and number of center zone (CZ) visits in PBS and CDS mice during the open field test. **(C)** Phase 1 (D = dummy object, M = unfamiliar mouse) and phase 2 (F = familiar mouse; N = novel mouse) of the social interaction test. The bar plots show the social preference index in phase 1 (values > 0 represent a preference towards M) and social memory index in phase 2 (values > 0 represent a preference towards N), whereas the line plots depict absolute exploration times in either phase. $^{\S}p < 0.001$, reflecting the overall main effect of object in phase 1 ($F_{(1,14)} = 29.8$); $^{\#}p < 0.05$, reflecting the overall main effect of object in phase 2 ($F_{(1,14)} = 5.9$). **(D)** The percentage bar plots depict the relative amount of time (%) exploring the left

(L) or right (R) object in sample phase 1 and 2 of the temporal order memory test. The bar plot shows the temporal order memory index during the test phase (values > 0 represent a preference towards the temporally more remote object presented in sample phase 1). All data are means ± SEM with individual values overlaid; $N = 8$ mice per group and test.

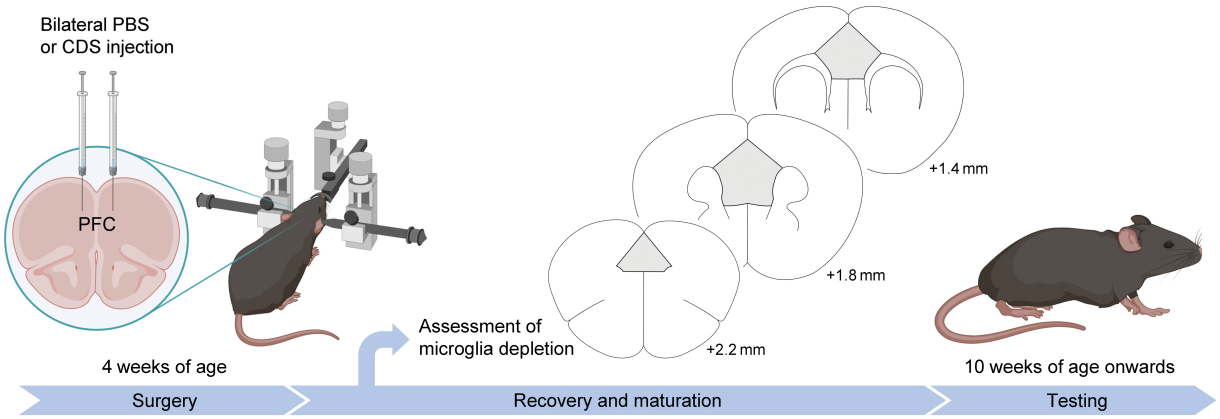

Fig. S23. Experimental design used to investigate the effects of transient microglia depletion in preadolescence. To deplete microglia selectively and transiently from the preadolescent prefrontal cortex, 4-week-old C57BL6/N male mice received a single, bilateral stereotaxic injection of CDS into the PFC. Control mice received a bilateral stereotaxic injection of PBS. The magnitude and specificity of microglia depletion was ascertained by post-mortem immunohistochemistry in the PFC (as highlighted by the gray area in the schematic coronal sections) at 1, 5 10 and 20 days post-injection (dpi) along the anterior (bregma +2.2. mm) to posterior (bregma +1.4 mm) axis. To test the effects of preadolescent microglia depletion on adult behavioral and cognitive functions, 4-week-old C57BL6/N male mice received a single, bilateral stereotaxic injection of CDS or PBS into PFC and were then allowed to recover for 6 weeks. A recovery period of 6 weeks was chosen to match the recovery and maturation period used in experiments, in which microglia were transiently depleted from the PFC of adolescent (see *figure S1*) or adult (see *figure S18*) mice. Hence, in the experimental setting of preadolescent microglia depletion, behavioral and cognitive testing commenced at 10 weeks of age.

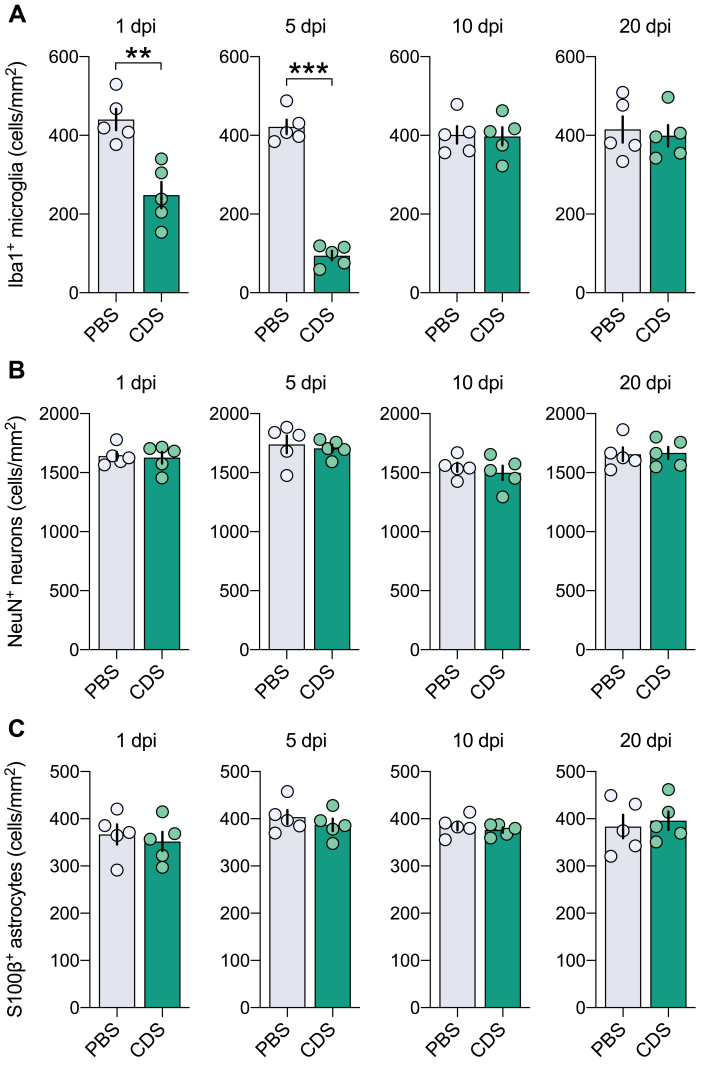

Fig. S24. Density of microglia, neurons and astrocytes in the PFC after PBS or CDS treatment in preadolescence. Post-mortem immunohistochemistry was used to assess whether bilateral, stereotaxic injection of CDS into the PFC of preadolescent male mice alters the density of microglia, neurons and astrocytes at 1, 5, 10 and 20 days post-injection (dpi). **(A)** Number of Iba1$^+$ microglia in the PFC of preadolescent PBS and CDS mice at the selected dpi. 1 dpi: $^{**}p < 0.01$ ($t_{(8)} = 4.2$); 5 dpi: $^{***}p < 0.001$ ($t_{(8)} = 15.1$). **(B)** Number of NeuN$^+$ neurons in the PFC of preadolescent PBS and CDS mice at the selected dpi. **(C)** Number of S100β$^+$ astrocytes in the PFC of preadolescent PBS and CDS mice at the selected dpi. All data are means ± SEM with individual values overlaid; $N = 5$ mice per group and dpi.

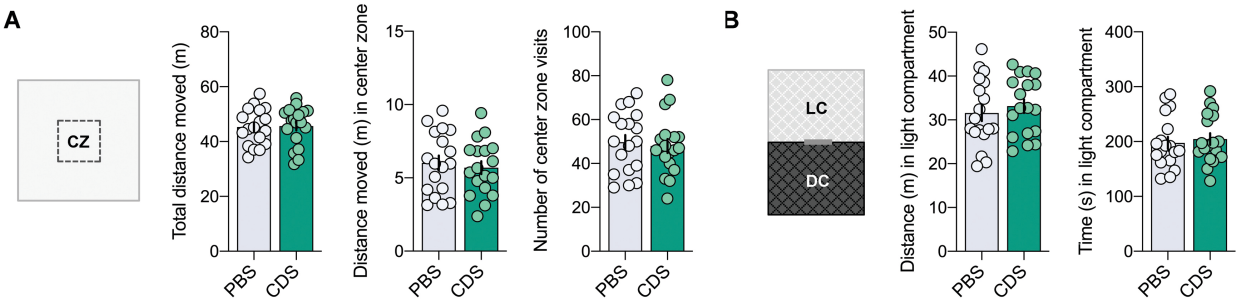

Fig. S25. Basal locomotor activity and anxiety-related behavior in adult mice subjected to PBS or CDS treatment in preadolescence. Male mice that received either a CDS or PBS injection during preadolescence were subjected to behavioral testing once they reached adulthood (see *figure S23*). **(A)** Total distance moved, distance moved in the center zone (CZ) and number of CZ visits in PBS and CDS mice during the open field test. **(B)** Distance moved and time spent in the light compartment (LC) in PBS and CDS mice during the light-dark box test, which measures the animals' exploration of the LC relative to the dark compartment (DC). All data are means ± SEM with individual values overlaid; $N = 18$ mice in each group and test.

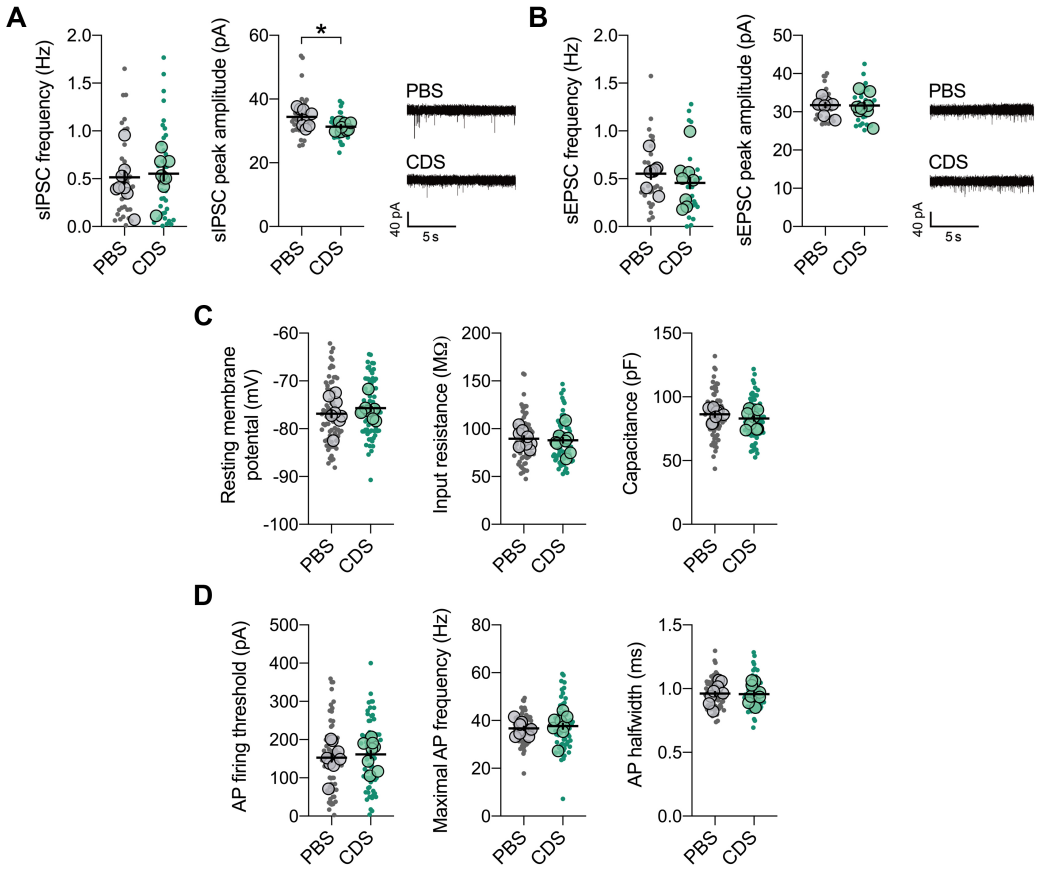

Fig. S26. Electrophysiological parameters of prefrontal pyramidal neurons after transient prefrontal microglia depletion in preadolescence. To test the effects of preadolescent microglia depletion on electrophysiological parameters of prefrontal pyramidal neurons in adulthood, 4-week-old C57BL6/N male mice received a single, bilateral stereotaxic injection of CDS or PBS into the PFC and were then allowed to recover and mature into adulthood (see *figure S23*). Electrophysiological recordings were conducted when the animals reached 10 weeks of age. **(A)** sIPSC frequency and peak amplitude of pyramidal neurons in the adult PFC of PBS and CDS mice. Dots represent individual cells (n = 33 cells from N = 8 mice per group), whereas filled circles reflect cell averages per animal. The picture shows representative sIPSC traces for PBS and CDS mice. **(B)** sEPSC frequency and peak amplitude of pyramidal neurons in the adult PFC of PBS and CDS mice. Dots represent individual cells (n = 28 for PBS, n = 29 for CDS; N = 8 mice per group), whereas filled circles reflect cell averages per animal. The picture shows representative sEPSC traces for PBS and CDS mice. **(C)** The scatter plots show measures of passive biophysical properties (resting membrane potential, input resistance and capacitance) in PBS and CDS mice. **(D)** The scatter plots depict measures of action potential (AP)-related properties (AP firing threshold and maximal AP frequency, AP half-width) in PBS and CDS mice. For all data**,** dots represent individual cells (n = 68 for PBS, n = 69 for CDS), whereas filled circles reflect cell averages per animal (N = 8 per group).

REFERENCES AND NOTES

1. E. Koechlin, C. Ody, F. Kouneiher, The architecture of cognitive control in the human prefrontal cortex. *Science* **302**, 1181–1185 (2003).

2. M. Carlén, What constitutes the prefrontal cortex? *Science* **358**, 478–482 (2017).

3. A. Caballero, R. Granberg, K. Y. Tseng, Mechanisms contributing to prefrontal cortex maturation during adolescence. *Neurosci. Biobehav. Rev.* **70**, 4–12 (2016).

4. M. Chini, I. L. Hanganu-Opatz, Prefrontal cortex development in health and disease: Lessons from rodents and humans. *Trends Neurosci.* **44**, 227–240 (2021).

5. B. Larsen, B. Luna Adolescence as a neurobiological critical period for the development of higher-order cognition. *Neurosci. Biobehav. Rev.* **94**, 179–195 (2018).

6. N. Gogtay, J. N. Giedd, L. Lusk, K. M. Hayashi, D. Greenstein, A. C. Vaituzis, T. F. Nugent, D. H. Herman, L. S. Clasen, A. W. Toga, J. Rapoport, P. M. Thompson, Dynamic mapping of human cortical development during childhood through early adulthood. *Proc. Natl. Acad. Sci. U.S.A.* **101**, 8174–8179 (2004).

7. T. Sakurai, N. J. Gamo, T. Hikida, S. H. Kim, T. Murai, T. Tomoda, A. Sawa Converging models of schizophrenia—Network alterations of prefrontal cortex underlying cognitive impairments. *Prog. Neurobiol.* **134**, 178–201 (2015).

8. L. D. Selemon, N. Zecevic, Schizophrenia: A tale of two critical periods for prefrontal cortical development. *Transl. Psychiatry* **5**, e623 (2015).

9. P. J. Harrison, L. Colbourne, C. H. Harrison, The neuropathology of bipolar disorder: Systematic review and meta-analysis. *Mol. Psychiatr.* **25**, 1787–1808 (2020).

10. S. A. Wolf, H. W. Boddeke, H. Kettenmann, Microglia in physiology and disease. *Annu. Rev. Physiol.* **79**, 619–643 (2017).

11. L. J. Lawson, V. H. Perry, P. Dri, S. Gordon, Heterogeneity in the distribution and morphology of microglia in the normal adult mouse brain. *Neuroscience* **39**, 151–170 (1990).

12. M. Mittelbronn, K. Dietz, H. J. Schluesener, R. Meyermann, Local distribution of microglia in the normal adult human central nervous system differs by up to one order of magnitude. *Acta Neuropathol.* **101**, 249–255 (2001).

13. D. P. Schafer, E. K. Lehrman, A. G. Kautzman, R. Koyama, A. R. Mardinly, R. Yamasaki, R. M. Ransohoff, M. E. Greenberg, B. A. Barres, B. Stevens, Microglia sculpt postnatal neural circuits in an activity and complement-dependent manner. *Neuron* **74**, 691–705 (2012).

14. A. R. Bialas, B. Stevens, Retracted article: TGF-β signaling regulates neuronal C1q expression and developmental synaptic refinement. *Nat. Neurosci.* **16**, 1773–1782 (2013).

15. L. Cheadle, S. A. Rivera, J. S. Phelps, K. A. Ennis, B. Stevens, L. C. Burkly, W. A. Lee, M. E. Greenberg, Sensory experience engages microglia to shape neural connectivity through a non-phagocytic mechanism. *Neuron* **108**, 451–468.e9 (2020).

16. L. Weinhard, G. di Bartolomei, G. Bolasco, P. Machado, N. L. Schieber, U. Neniskyte, M. Exiga, A. Vadisiute, A. Raggioli, A. Schertel, Y. Schwab, C. T. Gross, Microglia remodel synapses by presynaptic trogocytosis and spine head filopodia induction. *Nat. Commun.* **9**, 1228 (2018).

17. R. C. Paolicelli, G. Bolasco, F. Pagani, L. Maggi, M. Scianni, P. Panzanelli, M. Giustetto, T. A. Ferreira, E. Guiducci, L. Dumas, D. Ragozzino, C. T. Gross, Synaptic pruning by microglia is necessary for normal brain development. *Science* **333**, 1456–1458 (2011).

18. A. P. Mallya, H.-D. Wang, H. N. R. Lee, A. Y. Deutch, Microglial pruning of synapses in the prefrontal cortex during adolescence. *Cereb. Cortex* **29**, 1634–1643 (2019).

19. F. Ginhoux, M. Greter, M. Leboeuf, S. Nandi, P. See, S. Gokhan, M. F. Mehler, S. J. Conway, L. G. Ng, E. R. Stanley, I. M. Samokhvalov, M. Merad, Fate mapping analysis reveals that adult microglia derive from primitive macrophages. *Science* **330**, 841–845 (2010).

20. K. Kierdorf, D. Erny, T. Goldmann, V. Sander, C. Schul, E. G. Perdiguero, P. Wieghofer, A. Heinrich, P. Riemke, C. Hölscher, D. N. Müller, B. Luckow, T. Brocker, K. Debowski, G. Fritz, G. Opdenakker, A. Diefenbach, K. Biber, M. Heikenwalder, F. Geissmann, F. Rosenbauer, M. Prinz, Microglia emerge from erythromyeloid precursors via Pu.1- and Irf8-dependent pathways. *Nat. Neurosci.* **16**, 273–280 (2013).

21. C. N. Parkhurst, G. Yang, I. Ninan, J. N. Savas, J. R. Yates III, J. J. Lafaille, B. L. Hempstead, D. R. Littman, W. B. Gan, Microglia promote learning-dependent synapse formation through brain-derived neurotrophic factor. *Cell* **155**, 1596–609 (2013).

22. T. Masuda, L. Amann, R. Sankowski, O. Staszewski, M. Lenz, P. D. Errico, N. Snaidero, M. J. Costa Jordão, C. Böttcher, K. Kierdorf, S. Jung, J. Priller, T. Misgeld, A. Vlachos, M. Meyer-Luehmann, K. P. Knobeloch, M. Prinz, Novel Hexb-based tools for studying microglia in the CNS. *Nat. Immunol.* **21**, 802–815 (2020).

23. M. R. Elmore, A. R. Najafi, M. A. Koike, N. N. Dagher, E. E. Spangenberg, R. A. Rice, M. Kitazawa, B. Matusow, H. Nguyen, B. L. West, K. N. Green, Colony-stimulating factor 1 receptor signaling is necessary for microglia viability, unmasking a microglia progenitor cell in the adult brain. *Neuron* **82**, 380–397 (2014).

24. L. Torres, J. Danver, K. Ji, J. T. Miyauchi, D. Chen, M. E. Anderson, B. L. West, J. K. Robinson, S. E. Tsirka, Dynamic microglial modulation of spatial learning and social behavior. *Brain Behav. Immun.* **55**, 6–16 (2016).

25. P. P. Lehenkari, M. Kellinsalmi, J. P. Näpänkangas, K. V. Ylitalo, J. Mönkkönen, M. J. Rogers, A. Azhayev, H. K. Väänänen, I. E. Hassinen, Further insight into mechanism of action of clodronate: Inhibition of mitochondrial ADP/ATP translocase by a nonhydrolyzable, adenine-containing metabolite. *Mol. Pharmacol.* **61**, 1255–1262 (2002).

26. C. M. Drzewiecki, J. Willing, J. M. Juraska, Synaptic number changes in the medial prefrontal cortex across adolescence in male and female rats: A role for pubertal onset. *Synapse* **70**, 361–368 (2016).

27. L. K. Bicks, H. Koike, S. Akbarian, H. Morishita, Prefrontal cortex and social cognition in mouse and man. *Front. Psychol.* **6**, 1805 (2015).

28. G. R. Barker, F. Bird, V. Alexander, E. C. Warburton, Recognition memory for objects, place, and temporal order: A disconnection analysis of the role of the medial prefrontal cortex and perirhinal cortex. *J. Neurosci.* **27**, 2948–2957 (2007).

29. S. Maren, K. L. Phan, I. Liberzon, The contextual brain: Implications for fear conditioning, extinction and psychopathology. *Nat. Rev. Neurosci.* **14**, 417–428 (2013).

30. K. P. Berry, E. Nedivi, Spine dynamics: Are they all the same? *Neuron* **96**, 43–55 (2017).

31. G. Choii, J. Ko, Gephyrin: A central GABAergic synapse organizer. *Exp. Mol. Med.* **47**, e158 (2015).

32. J. M. Fritschy, H. Mohler, GABAA-receptor heterogeneity in the adult rat brain: Differential regional and cellular distribution of seven major subunits. *J. Comp. Neurol.* **359**, 154–194 (1995).

33. E. Bertoss, C. Tesini,A. Cappelli, E. Ciaramelli Ventromedial prefrontal damage causes a pervasive impairment of episodic memory and future thinking. *Neuropsychologia* **90**, 12–24 (2016).

34. O. Y. Chao, M. A. de Souza Silva, Y. M. Yang, J. P. Huston, The medial prefrontal cortex - hippocampus circuit that integrates information of object, place and time to construct episodic memory in rodents: Behavioral, anatomical and neurochemical properties. *Neurosci. Biobehav. Rev.* **113**, 373–407 (2020).

35. B. Delatour, P. Gisquet-Verrier, Involvement of the dorsal anterior cingulate cortex in temporal behavioral sequencing: Subregional analysis of the medial prefrontal cortex in rat. *Behav. Brain Res.* **126**, 105–114 (2001).

36. D. K. Hannesson, G. Vacca, J. G. Howland, A. G. Phillips, Medial prefrontal cortex is involved in spatial temporal order memory but not spatial recognition memory in tests relying on spontaneous exploration in rats. *Behav. Brain Res.* **153**, 273–285 (2004).

37. N. M. Dudukovic, A. D. Wagner, Goal-dependent modulation of declarative memory: Neural correlates of temporal recency decisions and novelty detection. *Neuropsychologia* **45**, 2608–2620 (2007).

38. A. Caballero, E. Flores-Barrera, D. K. Cass, K. Y. Tseng, Differential regulation of parvalbumin and calretinin interneurons in the prefrontal cortex during adolescence. *Brain Struct. Funct.* **219**, 395–406 (2014).

39. D. K. Cass, E. Flores-Barrera, D. R. Thomases, W. F. Vital, A. Caballero, K. Y. Tseng, CB1 cannabinoid receptor stimulation during adolescence impairs the maturation of GABA function in the adult rat prefrontal cortex. *Mol. Psychiatry* **19**, 536–543 (2014).

40. J. H. Kim, R. Richardson, A developmental dissociation of context and GABA effects on extinguished fear in rats. *Behav. Neurosci.* **121**, 131–139 (2007).

41. J. H. Kim, A. S. Hamlin, R. Richardson, Fear extinction across development: The involvement of the medial prefrontal cortex as assessed by temporary inactivation and immunohistochemistry. *J. Neurosci.* **29**, 10802–10808 (2009).

42. E. C. King, S. S. Pattwell, C. E. Glatt, F. S. Lee, Sensitive periods in fear learning and memory. *Stress* **17**, 13–21 (2014).

43. M. G. Cunningham, S. Bhattacharyya, F. M. Benes, Amygdalo-cortical sprouting continues into early adulthood: Implications for the development of normal and abnormal function during adolescence. *J. Comp. Neurol.* **453**, 116–130 (2002).

44. T. Chan, K. Kyere, B. R. Davis, A. Shemyakin, P. A. Kabitzke, H. N. Shair, G. A. Barr, C. P. Wiedenmayer, The role of the medial prefrontal cortex in innate fear regulation in infants, juveniles, and adolescents. *J. Neurosci.* **31**, 4991–4999 (2011).

45. A. Waisman, F. Ginhoux, M. Greter, J. Bruttger, Homeostasis of microglia in the adult brain: Review of novel microglia depletion systems. *Trends Immunol.* **36**, 625–636 (2015).

46. R. Hanamsagar, M. D. Alter, C. S. Block, H. Sullivan, J. L. Bolton, S. D. Bilbo, Generation of a microglial developmental index in mice and in humans reveals a sex difference in maturation and immune reactivity. *Glia* **65**, 1504–1520 (2017).

47. V. Mondelli, A. C. Vernon, F. Turkheimer, P. Dazzan, C. M. Pariante, Brain microglia in psychiatric disorders. *Lancet Psychiatry* **4**, 563–572 (2017).

48. E. Parellada, P. Gassó, Glutamate and microglia activation as a driver of dendritic apoptosis: A core pathophysiological mechanism to understand schizophrenia. *Transl. Psychiatry* **11**, 271 (2021).

49. M. Germann, S. G. Brederoo, I. E. C. Sommer, Abnormal synaptic pruning during adolescence underlying the development of psychotic disorders. *Curr. Opin. Psychiatry* **34**, 222–227 (2021).

50. M. S. Keshavan, J. Giedd, J. Y. Lau, D. A. Lewis, T. Paus, Changes in the adolescent brain and the pathophysiology of psychotic disorders. *Lancet Psychiatry* **1**, 549–558 (2014).

51. T. Notter, S. M. Schalbetter, N. E. Clifton, D. Mattei, R. Richetto, K. Thomas, U. Meyer, J. Hall, Neuronal activity increases translocator protein (TSPO) levels. *Mol. Psychiatry* **26**, 2025–2037 (2021).

52. M. Schalbetter, F. S. Mueller, J. Scarborough, J. Richetto, U. Weber-Stadlbauer, U. Meyer, T. Notter, Oral application of clozapine-N-oxide using the micropipette-guided drug administration (MDA) method in mouse DREADD systems. *Lab. Anim* **50**, 69–75 (2021).

53. M. A. Labouesse, W. Langhans, U. Meyer, Abnormal context-reward associations in an immune-mediated neurodevelopmental mouse model with relevance to schizophrenia. *Transl. Psychiatry* **5**, e637 (2015).

54. J. Richetto, M. A. Labouesse, M. M. Poe, J. M. Cook, A. A. Grace, M. A. Riva, U. Meyer, Behavioral effects of the benzodiazepine-positive allosteric modulator SH-053-2'F-S-CH_3 in an immune-mediated neurodevelopmental disruption model. *Int. J. Neuropsychopharmacol.* **18**, pyu055 (2015).

55. U. Weber-Stadlbauer, J. Richetto, M. A. Labouesse, J. Bohacek, I. M. Mansuy, U. Meyer, Transgenerational transmission and modification of pathological traits induced by prenatal immune activation. *Mol. Psychiatry* **22**, 102–112 (2017).

56. F. S. Mueller, J. Scarborough, S. M. Schalbetter, J. Richetto, E. Kim, A. Couch, Y. Yee, J. P. Lerch, A. C. Vernon, U. Weber-Stadlbauer, U. Meyer, Behavioral, neuroanatomical, and molecular correlates of resilience and susceptibility to maternal immune activation. *Mol. Psychiatry* **26**, 396–410 (2021).

57. C. Belzung, G. Griebel. Measuring normal and pathological anxiety-like behaviour in mice: A review. *Behav. Brain Res.* **125**, 141–149 (2001).

58. T. Notter, J. M. Coughlin, T. Gschwind, U. Weber-Stadlbauer, Y. Wang, M. Kassiou, A. C. Vernon, D. Benke, M. G. Pomper, A. Sawa, U. Meyer, Translational evaluation of translocator protein as a marker of neuroinflammation in schizophrenia. *Mol. Psychiatry* **23**, 323–334 (2018).

59. T. Notter, P. Panzanelli, S. Pfister, D. Mircsof, J. M. Fritschy, A protocol for concurrent high-quality immunohistochemical and biochemical analyses in adult mouse central nervous system. *Eur. J. Neurosci.* **39**, 165–175 (2014).

60. K. E. Binley, W. S. Ng, J. R. Tribble, B. Song, J. E. Morgan, Sholl analysis: A quantitative comparison of semi-automated methods. *J. Neurosci. Methods* **225**, 65–70 (2014).

61. A. Dobin, C. A. Davis, F. Schlesinger, J. Drenkow, C. Zaleski, S. Jha, P. Batut, M. Chaisson, T. R. Gingeras, STAR: Ultrafast universal RNA-seq aligner. *Bioinformatics* **29**, 15–21 (2013).

62. Y. Liao, G. K. Smyth, W. Shi, featureCounts: An efficient general purpose program for assigning sequence reads to genomic features. *Bioinformatics* **30**, 923–930 (2014).

63. M. I. Love, W. Huber, S. Anders, Moderated estimation of fold change and dispersion for RNA-seq data with DESeq2. *Genome Biol.* **15**, 550 (2014).

64. G. Yu, L. G. Wang, Y. Han, Q. Y. He, clusterProfiler: An R package for comparing biological themes among gene clusters. *OMICS* **16**, 284–287 (2012).

65. S. Thomas, D. Bonchev, A survey of current software for network analysis in molecular biology. *Hum. Genomics* **4**, 353–360 (2010).

66. D. Mattei, A. Ivanov, M. van Oostrum, S. Pantelyushin, J. Richetto, F. Mueller, M. Beffinger, L. Schellhammer, J. Vom Berg, B. Wollscheid, D. Beule, R. C. Paolicelli, U. Meyer, Enzymatic dissociation induces transcriptional and proteotype bias in brain cell populations. *Int. J. Mol. Sci.* **21**, 7944 (2020).

67. K. J. Livak, T. D. Schmittgen, Analysis of relative gene expression data using real-time quantitative PCR and the 2−ΔΔCT method. *Methods* **25**, 402–408 (2001).

68. J. D. Cahoy, B. Emery, A. Kaushal, L. C. Foo, J. L. Zamanian, K. S. Christopherson, Y. Xing, J. L. Lubischer, P. A. Krieg, S. A. Krupenko, W. J. Thompson, B. A. Barres, A transcriptome database for astrocytes, neurons, and oligodendrocytes: A new resource for understanding brain development and function. *J. Neurosci.* **28**, 264–278 (2008).

69. Y. Zhang, K. Chen, S. A. Sloan, M. L. Bennett, A. R. Scholze, S. O'Keeffe, H. P. Phatnani, P. Guarnieri, C. Caneda, N. Ruderisch, S. Deng, S. A. Liddelow, C. Zhang, R. Daneman, T. Maniatis, B. A. Barres, J. Q. Wu, An RNA-sequencing transcriptome and splicing database of glia, neurons, and vascular cells of the cerebral cortex. *J. Neurosci.* **34**, 11929–11947 (2014).

70. T. R. Hammond, C. Dufort, L. Dissing-Olesen, S. Giera, A. Young, A. Wysoker, A. J. Walker, F. Gergits, M. Segel, J. Nemesh, S. E. Marsh, A. Saunders, E. Macosko, F. Ginhoux, J. Chen, R. J. M. Franklin, X. Piao, S. A. McCarroll, B. Stevens, Single-cell RNA sequencing of microglia throughout the mouse lifespan and in the injured brain reveals complex cell-state changes. *Immunity* **50**, 253–271 (2019).